A Two-Level Primitive Equation Atmospheric Model Designed for Climatic Sensitivity Experiments[1]

ISAAC M. HELD

Center for Earth and Planetary Physics, Harvard University, Cambridge, Mass. 02138

MAX J. SUAREZ

Department of Atmospheric Sciences, University of California, Los Angeles 90024

(Manuscript received 9 June 1977, in final form 17 October 1977)

ABSTRACT

A useful but as yet under-utilized tool for climatic studies is an atmospheric model in which the time evolution of large-scale eddies is resolved explicitly, but in a relatively simple dynamical framework. One such model is described in detail in this study—a two-level primitive equation model on a sphere with variable static stability, finite-differenced in the meridional direction but Fourier analyzed and then very severely truncated in the zonal direction. Two versions of the model—moist and dry—are developed, the maintenance of the model's static stability being markedly different in the two versions.

Statistically steady states are obtained for a variety of spectral truncations for both versions of the model in order to determine the fewest zonal wavenumbers one can retain and still obtain a reasonable zonally averaged circulation. Including only one wave, of wavelength typical of strongly unstable waves in mid-latitudes, results in a circulation with a subpolar jet as well as a subtropical jet in the zonal wind. The addition of a longer wave (i.e., the addition of wavenumber 3 to wavenumber 6) results in the destruction of the subpolar jet. No further dramatic changes in the zonally averaged flow occur as more waves are added to the system.

Features of the model's dynamics which might limit its utility are emphasized, notably the dependence of the strength of the Hadley cell on the details of the convective adjustment scheme. We find, however, that the total energy transported by the Hadley cell is insensitive to such details.

Climatic sensitivity experiments with these models will be described in forthcoming papers.

1. Introduction

Estimates of climatic sensitivity have, to date, been based on climate models of very disparate types. On the one hand, a variety of valuable calculations have been based on models which treat the effects of atmospheric dynamics in only the most cursory way. Some examples are the energy balance calculations of Budyko (1969) and Sellers (1969) and the radiative-convective equilibrium models of Manabe and Strickler (1964), Manabe and Wetherald (1967) and Ramanathan (1976). On the other hand, a few sensitivity studies have been conducted with general circulation models of the atmosphere (Wetherald and Manabe, 1975; Gates, 1976). Much work is clearly needed with models of intermediate complexity in order to appreciate the limitations of the simple energy balance and radiative-convective formulations, and in order to help understand and evaluate the results generated by general circulation models.

The usefulness of any such intermediate atmospheric model will be determined to a great extent by the validity of its treatment of the large-scale eddy fluxes of heat, momentum and moisture. The "parameterization" of these fluxes, their incorporation into models of the atmospheric circulation without resolving the time evolution of individual eddies, is certainly a problem of utmost importance for climate modeling. Parameterization schemes have been incorporated into atmospheric models by various workers (Kurihara, 1970; Sela and Wiin-Nielsen, 1971; Webster and Lau, 1977). Although of considerable interest, these schemes are not based on any convincing dynamical theories. For some purposes, however, it may be possible to avoid this difficult problem by developing a model with sufficiently few degrees of freedom that its climatic statistics are easily obtained, which nevertheless predicts the time evolution of those eddies responsible for the bulk of the transports. We have tried to develop a model of this sort. Despite its limitations, we believe it to be a useful tool for gaining insights into the gross response of atmospheric dynamics to perturbations in external parameters.

The dynamical framework we have chosen is that of a two-level primitive equation model on a sphere. The equations are Fourier analyzed and then *very* severely

[1] Most of the work presented in this paper was completed while the authors were students in the Geophysical Fluid Dynamics Program, Princeton University.

0022-4928/78/0206-0229$12.00

truncated in the zonal direction, finite-differenced in the meridional direction and integrated semi-implicitly in time. [Meridional finite-differencing combined with zonal Fourier decomposition is not uncommon in atmospheric modeling. An example is Bates (1970).] In this paper, the first part of a continuing study, we describe the model in detail, emphasizing the manner in which those few zonal wavenumbers retained in the computations have been chosen.

Our purpose in constructing and analyzing such a model is not to compete with larger models in simulating the general circulation or in estimating climatic sensitivity. The severe spectral truncation and semi-implicit time integration allow us to adequately define statistically steady states with relative ease, yet the model produces a circulation resembling in its broad features that of the atmosphere. Climatic responses can be studied in a relatively simple dynamical context and compared with responses in other models.

Two versions of the model are developed. In the "moist" version, water vapor mixing ratio is a prognostic variable in the lower layer, and a moist convective adjustment does not allow a saturated atmosphere to become less stable than a moist adiabat. In the "dry" version, water vapor is not transported by atmospheric motions, and the model atmosphere is allowed to approach the dry adiabat. The maintenance of the model's static stability is, needless to say, very different in these two versions.

Our prescription for convective adjustment in the moist version involves an arbitrary choice of a precipitation criterion. The effect of different choices of this parameter on the model's tropical climate is analyzed briefly. The insensitivity of tropical temperatures to the strength of the predicted tropical circulation is of particular interest.

In forthcoming papers, we shall describe how both moist and dry versions of the model respond to variations in the solar intensity with fixed surface albedos and fixed cloudiness. The importance of the response of the static stability for the sensitivity of surface temperatures and eddy fluxes will be analyzed and comparisons made with several parameterization schemes. We shall also describe sensitivity experiments in which surface albedos are taken to be a simple function of surface temperature, and compare these results with the predictions of energy balance models similar to those of Budyko and Sellers.

2. The moist model

We begin by describing the moist model. The differences between the moist and dry models are summarized in Section 3.

We choose a two-level model as the simplest framework in which baroclinic eddies can be represented. Since the response of the tropospheric static stability may well be an important aspect of climatic responses of interest, we consider a model which predicts potential temperature as well as horizontal velocity at each of two levels in the vertical. The vertical finite-differencing used is essentially that discussed by Lorenz (1960).

TABLE 1. The notation and the values used for several of the physical constants required by the model.

Constant	Symbol	Value
Radius of the earth	a	6.4×10^{6} m
Rotation rate of the earth	Ω	$2\pi/(8.64\times10^{4})$ s^{-1}
Heat capacity of air per unit mass at constant pressure	c_p	10^{3} m s^{-2} °C^{-1}
Acceleration due to gravity	g	9.8 m s^{-2}
Latent heat of vaporization of water	L	2.5×10^{6} J kg^{-1}
Stefan-Boltzmann constant	σ	5.67×10^{-8} W m^{-2} K^{-4}

Since balanced models with variable static stability on a sphere offer no great computational advantages over the primitive equations integrated with a semi-implicit time step, the latter alternative is chosen. The equations are further simplified by setting the vertically averaged divergence of the flow equal to zero, as in Smagorinsky (1963). The two levels at which horizontal velocities and potential temperatures are predicted are chosen to be $p_1=250$ mb and $p_2=750$ mb. (The subscripts 1 and 2 hereafter refer to the upper and lower levels, respectively.) Given any variable ρ defined at the upper and lower levels, we use the notation

$$\bar{\rho}\equiv\tfrac{1}{2}(\rho_1+\rho_2) \quad \text{and} \quad \hat{\rho}\equiv\tfrac{1}{2}(\rho_1-\rho_2).$$

We define

$$A\equiv\overline{(p/p_*)^{\kappa}}=0.797,$$

$$B\equiv-\widehat{(p/p_*)^{\kappa}}=0.124,$$

where $p_*\equiv1000$ mb, $\kappa\equiv(\gamma-1)/\gamma$ and $\gamma\equiv c_p/c_v$, c_p and c_v being the heat capacities per unit mass of air at constant pressure and volume.

The hydrostatic relation $\partial\phi/\partial(p/p_*)^{\kappa}=-c_p\Theta$, is given the finite-differenced form $\hat{\phi}=c_pB\bar{\Theta}$, where ϕ is the geopotential and Θ the potential temperature. Our model can then be written as six prognostic equations—for the baroclinic zonal and meridional velocities, the barotropic vorticity, the mean atmospheric potential temperature and static stability, and the water vapor mixing ratio in the lower layer—

$$\frac{\partial\hat{u}}{\partial t}=2\Omega\sin(\theta)\hat{v}-\frac{c_pB}{a\cos(\theta)}\frac{\partial\bar{\Theta}}{\partial\lambda}-\nabla_H\cdot\widehat{(\mathbf{v}u)}-\omega\bar{u}+\frac{\tan(\theta)}{a}\widehat{uv}+\hat{F}^{\lambda}, \quad (1)$$

$$\frac{\partial\hat{v}}{\partial t}=-2\Omega\sin(\theta)\hat{u}-\frac{c_pB}{a}\frac{\partial\bar{\Theta}}{\partial\theta}-\nabla_H\cdot\widehat{(\mathbf{v}v)}-\omega\bar{v}-\frac{\tan(\theta)}{a}\widehat{u^2}+\hat{F}^{\theta},$$

$$\frac{\partial\zeta}{\partial t}=-\frac{2\Omega\cos(\theta)}{a}\bar{v}+\frac{1}{a\cos(\theta)}\frac{\partial}{\partial\lambda}\times\left(-\nabla_H\cdot(\overline{\mathbf{v}v})-\frac{\tan(\theta)}{a}\overline{u^2}+\bar{F}^\theta\right)-\frac{1}{a\cos(\theta)}\frac{\partial}{\partial\theta}\times\left(\cos(\theta)\left[-\nabla_H\cdot(\overline{\mathbf{v}u})+\frac{\tan(\theta)}{a}\overline{uv}+\bar{F}^\lambda\right]\right),$$

$$\frac{\partial\bar{\Theta}}{\partial t}=-\nabla_H\cdot(\overline{\mathbf{v}\Theta})+\frac{1}{c_p}\overline{\left(\frac{p_*}{p}\right)^\kappa Q},$$

$$\frac{\partial\hat{\Theta}}{\partial t}=-\nabla_H\cdot(\widehat{\mathbf{v}\Theta})-\omega\bar{\Theta}+\frac{1}{c_p}\widehat{\left(\frac{p_*}{p}\right)^\kappa Q},$$

$$\frac{\partial r}{\partial t}=-\nabla_H\cdot(\mathbf{v}_2 r)+W,$$

and the diagnostic continuity equation

$$\omega=-\nabla_H\cdot\hat{\mathbf{v}}.$$

In (1), θ, λ and t represent latitude, longitude and time, $\mathbf{v}=(u,v)$ is the horizontal velocity, ω the vertical p-velocity at 500 mb divided by $\Delta p\equiv 500$ mb, and r the water vapor mixing ratio in the lower layer. The mixing ratio in the upper layer is set equal to zero and advection of water vapor across 500 mb is ignored. All information about the vertically averaged flow is carried by its vorticity ζ or its streamfunction ψ,

$$\zeta\equiv\frac{1}{a^2\cos(\theta)}\frac{\partial}{\partial\theta}[\cos(\theta)\partial\psi/\partial\theta]+\frac{1}{a^2\cos^2(\theta)}\partial^2\psi/\partial\lambda^2,$$

$$\bar{u}\equiv-\frac{1}{a}\partial\psi/\partial\theta,$$

$$\bar{v}\equiv\frac{1}{a\cos(\theta)}\partial\psi/\partial\lambda.$$

$\nabla_H\cdot(\ )$ is the horizontal divergence operator, i.e.,

$$\nabla_H\cdot\bar{\mathbf{v}}=\frac{1}{a\cos(\theta)}\frac{\partial\bar{u}}{\partial\lambda}+\frac{1}{a\cos(\theta)}\frac{\partial}{\partial\theta}[\cos(\theta)\bar{v}]\equiv 0.$$

$\mathbf{F}=(F^\lambda,F^\theta)$ is the frictional force per unit mass, Q the diabatic heating per unit mass, and W the source of water vapor mixing ratio. Values of the parameters in (1) appropriate for the earth and the values of other physical constants we shall need are listed in Table 1.

We assume a zonally symmetric earth so that there can be no longitudinal structure in the model's climate. (Without denying the possibly great importance of standing eddies in climatic problems, we feel that some understanding of zonally symmetric responses is a natural prerequisite for the study of the zonally asymmetric system.) It then seems reasonable to utilize as many of the available degrees of freedom as possible in describing latitudinal climatic variations. We therefore Fourier analyze all fields in the zonal direction and experiment with various severe spectral truncations.

In those experiments in which only one wave interacting with the zonal flow is retained, all fields are assumed to be of the form

$$Z(\lambda,\theta)=z_0(\theta)+z_m e^{im\lambda}+z_m^* e^{-im\lambda}$$

and all nonlinear products $Z=XY$ in the model equations are replaced by

$$\begin{cases} z_0=x_0y_0+2\ \mathrm{Re}(x_m y_m^*) \\ z_m=x_m y_0+x_0 y_m. \end{cases}$$

In those experiments in which more than one wave is retained, we always choose a set of wavenumbers that are consecutive multiples of some fundamental wavenumber M so as to allow the maximum amount of nonlinear interaction. If n waves are retained, all fields are assumed to take the form

$$Z(\lambda,\theta)=\sum_{l=-n}^{n} z_{lM}(\theta)e^{ilM\lambda},\quad (z_{-m}=z_m^*)$$

and nonlinear products are replaced by

$$z_{lM}=\sum_{l'l''}{}' x_{l'M}y_{l''M}, \tag{2}$$

where the primed summation is over all pairs of integers (l',l'') such that $|l'|,\ |l''|\leqslant n$ and $l'+l''=l$.

In the meridional direction the variables are placed on a staggered grid to help avoid two-grid interval noise and to simplify the use of a semi-implicit time-step. The grid is depicted in Fig. 1. The polar boundaries, across which the resolved and diffusive fluxes of heat, momentum and moisture are all identically zero, are placed at 84°N and 84°S. Since we do not include wavenumbers 1 and 2 in any of our computations, there is little purpose in extending the integrations to the poles. The grid size Δ is 3° latitude.

The numerical scheme is designed to conserve (for inviscid, adiabatic flow) finite-difference analogs of mean potential temperature, mean-square potential temperature, total energy, available potential plus kinetic energy and relative angular momentum. The meridional finite-differencing is similar to that used by Bryan (1969) in a numerical ocean model. The time

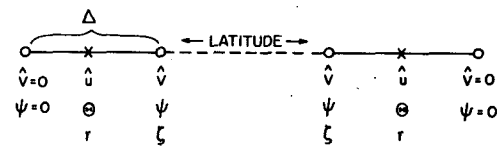

FIG. 1. The staggered grid used for the meridional finite-differencing.

finite-differencing follows Kwizak and Robert (1971) in treating advective terms explicitly and terms responsible for gravitational oscillations implicitly, except that we treat the Coriolis force implicitly as well. Details of both the space and time finite-differencing are presented in the Appendix.

The forcing functions used in our calculations can be written in the form

$$\mathbf{F}_1=\mathbf{F}_1^{\text{diff}},$$
$$\mathbf{F}_2=\mathbf{F}_2^{\text{diff}}+\mathbf{F}^{\text{surf}},$$
$$Q_1=Q_1^{\text{rad}}+Q_1^{\text{diff}}+Q^{\text{conv}},$$
$$Q_2=Q_2^{\text{rad}}+Q_2^{\text{diff}}+Q^{\text{sh}}+LP-Q^{\text{conv}},$$
$$W=W^{\text{evap}}+W^{\text{diff}}-P.$$

The frictional force in the upper layer consists solely of a lateral diffusion. In the lower layer, there is a surface stress in addition to lateral diffusion. The upper layer is heated by short- and longwave radiation, by the lateral diffusion of heat, and by the heat released by a convective adjustment. The lower layer is heated by short- and longwave radiation, lateral diffusion, sensible heat flux from the surface and by latent heat release, and is cooled by the heat transferred upward by the convective adjustment. Heat released upon the frictional dissipation of kinetic energy is ignored. Evaporation provides a source of water vapor which is also diffused and lost through precipitation.

Several of these forcing terms take different forms in the zonal and eddy equations. Each of them is discussed in turn below.

a. Radiative heating

Eddy temperatures are simply damped linearly

$$\left(\frac{p_*}{p}\right)^{\kappa} Q_{k,m}^{\text{rad}}=-c_p\Theta_{k,m}/\tau_R \quad (m\neq 0),$$

with a radiative decay time τ_R of 20 days. (Whenever two subscripts appear on the same symbol, the first refers to the level and the second to the zonal wavenumber.)

In the zonally averaged thermodynamic equation, the calculation of longwave cooling rates is based on that of Rodgers and Walshaw (1966), as modified by Stone and Manabe (1968). The short wave calculation is based on that described in Manabe and Strickler (1964). To utilize these models we assume a temperature profile linear in the logarithm of pressure from the surface to 200 mb, isothermal above 200 mb, and passing through the two predicted temperatures

$$T_1=(\tfrac{1}{4})^{\kappa}\Theta_1 \quad \text{and} \quad T_2=(\tfrac{3}{4})^{\kappa}\Theta_2$$

at 250 and 750 mb (see Fig. 2). The *relative* humidity is assumed to be a given function of pressure and independent of latitude and time; cloud heights, amounts

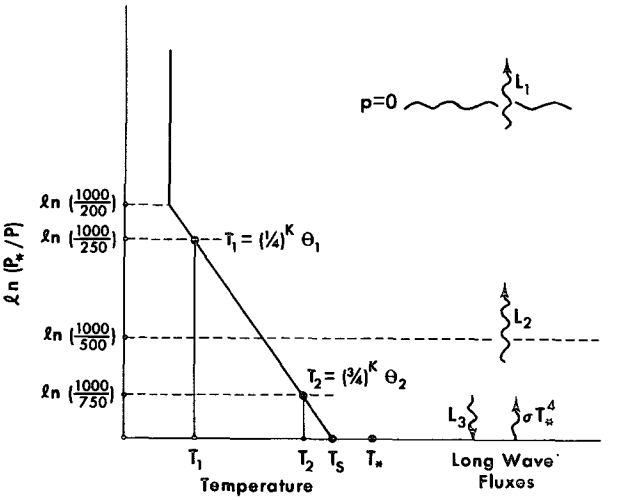

FIG. 2. The temperature profile used in the computation of long- and shortwave heating rates, and a schematic of the longwave fluxes derived from these computations.

and albedos are fixed independent of latitude and time; and the carbon dioxide mixing ratio is fixed independent of latitude, pressure and time—all at the values used by Manabe and Wetherald (1967). Absorption by ozone is ignored. (The relative humidity profile and cloud amounts utilized in these radiative calculations are independent of the predicted hydrologic cycle described below.)

The upward flux of longwave radiation at the top of the atmosphere, L_1, the net longwave flux at 500 mb, L_2, and the downward longwave flux at the surface L_3 predicted by the radiative model can be thought of as functions of $\bar{\Theta}_0$, $\hat{\Theta}_0$ and $\Delta T\equiv T_*-T_s$, where T_* is the surface temperature and T_s the atmospheric temperature at the surface (see Fig. 2)

$$T_s\equiv\bar{T}_0-1.522\hat{T}_0$$
$$=0.986\bar{\Theta}_0-1.337\hat{\Theta}_0.$$

Since $\hat{\Theta}_0$ and ΔT do not vary over large ranges in our calculations (compared with variations in $\bar{\Theta}_0$), we use least-square fits of the form

$$L_i=a_i(\bar{\Theta}_0)+b_i(\bar{\Theta}_0)\hat{\Theta}_0+c_i(\bar{\Theta}_0)\Delta T.$$

The functions a_i, b_i and c_i are presented in Table 2. ($c_3=0$ since L_3 does not depend on T_*.) The longwave heating of the upper layer is then $(L_2-L_1)g/\Delta p$, and the longwave heating of the lower layer

$$(\sigma T_*^4-L_3-L_2)g/\Delta p.$$

The shortwave heating rates predicted by the radiative model are functions of the incident flux, its zenith angle, the two zonally averaged atmospheric temperatures and the surface albedo. These heating rates are approximated by a procedure similar to that used for the longwave heating rates. As the detailed

TABLE 2. The parameters a_i, b_i and c_i used in the computation of longwave heating rates. a_1, a_2 and a_3 are in units of W m^{-2}; b_1, b_2, b_3, c_1 and c_2 are in units of W (m^2 °C)$^{-1}$.

$\bar{\Theta}$(°C)	a_1	b_1	c_1	a_2	b_2	c_2	a_3	b_3
−30	109.0	−1.10	1.00	121.3	−2.18	1.26	104.3	1.62
−25	118.0	−1.16	1.01	131.0	−2.29	1.25	119.1	1.95
−20	127.4	−1.22	1.01	140.8	−2.28	1.25	134.7	2.25
−15	136.9	−1.26	1.01	150.6	−2.47	1.25	150.9	2.51
−10	146.8	−1.30	1.01	160.0	−2.52	1.26	167.8	2.75
− 5	156.8	−1.34	1.01	168.3	−2.55	1.26	185.7	3.00
0	167.2	−1.37	1.01	176.4	−2.60	1.26	204.9	3.25
5	177.6	−1.40	1.01	183.7	−2.64	1.25	225.7	3.54
10	188.3	−1.42	0.99	190.6	−2.68	1.24	248.1	3.85
15	199.2	−1.43	0.97	197.0	−2.72	1.21	271.9	4.17
20	210.0	−1.44	0.95	202.8	−2.74	1.18	281.1	4.49
25	221.0	−1.44	0.92	208.1	−2.75	1.15	306.2	4.81
30	232.1	−1.43	0.88	213.1	−2.76	1.10	332.9	5.15
35	243.2	−1.41	0.83	217.6	−2.75	1.04	361.8	5.54
40	254.2	−1.39	0.77	221.7	−2.73	0.96	393.3	5.98
45	265.0	−1.35	0.68	225.0	−2.69	0.85	427.7	6.48
50	275.6	−1.30	0.59	227.8	−2.65	0.74	465.0	7.03
55	286.1	−1.24	0.48	230.2	−2.60	0.61	504.9	7.60
60	296.2	−1.16	0.39	231.9	−2.53	0.48	547.1	8.19
65	306.0	−1.08	0.30	233.0	−2.45	0.37	591.1	8.75
70	315.6	− .98	0.24	233.6	−2.36	0.29	636.0	9.26

disposition of the shortwave flux has little bearing on the discussion of model results in this paper, we refer the interested reader to Suarez (1976) or to Held (1976) for these details.

Incident solar radiation is given its annual mean values as a function of latitude. The solar constant is set at 1360 W m^{-2}, and surface albedoes are fixed at 0.10 independent of latitude. Typically, ~6% of the globally averaged incident flux is absorbed in the upper layer, ~14% in the lower layer, and ~46% at the surface.

b. *Convection and precipitation*

Having little confidence in the two-level model's ability to simulate the tropical atmosphere, we try to design a scheme for convective adjustment and precipitation that will produce a steady, zonally symmetric tropical circulation free of disturbances forced by latent heat release.

Given a moist adiabatic temperature profile, one can calculate

$$\bar{T}=\tfrac{1}{2}[(p_1/p_*)^\kappa\Theta_1+(p_2/p_*)^\kappa\Theta_2],$$
$$\Theta_{\text{crit}}=\tfrac{1}{2}(\Theta_1-\Theta_2),$$

from the temperatures at 250 and 750 mb. One can then think of $\hat{\Theta}_{\text{crit}}$ as a function of $\bar{T}$. The function thus obtained is plotted in Fig. 3. We refer to $\hat{\Theta}_{\text{crit}}(\bar{T})$ as the static stability of the moist adiabatic profile in an atmosphere with mean temperature $\bar{T}$. When "moist convection" is occurring in the model we assume that $\hat{\Theta}=\hat{\Theta}_{\text{crit}}$.

It follows from (1) in the special case of inviscid, adiabatic flow that

$$c_p\frac{\partial\bar{T}}{\partial t}+\tfrac{1}{2}c_p\nabla_H\cdot[\mathbf{v}_1(\bar{T}+A\hat{\Theta})+\mathbf{v}_2(\bar{T}-A\hat{\Theta})]$$
$$=-c_pB\hat{\mathbf{v}}\cdot\nabla_H\bar{\Theta}. \quad (3)$$

The right-hand side of (3) is the conversion of potential plus internal into kinetic energy. We therefore recognize $c_p(\bar{T}+A\hat{\Theta})$ and $c_p(\bar{T}-A\hat{\Theta})$ as the finite-difference analogs of dry static energy in the upper and lower layers. The natural analogs of moist static energy in the model are then $\mathcal{H}_1\equiv c_p(\bar{T}+A\hat{\Theta})$ in the upper layer (where there is no water vapor) and $\mathcal{H}_2\equiv c_p(\bar{T}-A\hat{\Theta})+Lr$ in the lower layer. If we neglect the small transport of kinetic energy, the poleward energy transport by a steady, zonally symmetric circulation is proportional to

$$v_{1,0}\mathcal{H}_1-v_{2,0}\mathcal{H}_2=v_{1,0}(\mathcal{H}_1-\mathcal{H}_2)$$
$$=v_{1,0}(2c_pA\hat{\Theta}_0-Lr_0).$$

(Although the lower tropical atmosphere is observed to be conditionally unstable, the atmosphere must be conditionally stable "in the large"—the average moist static energy in the poleward flow aloft must be larger than the average moist static energy in the equatorward flow in the lower troposphere—if the Hadley cell is to transport energy poleward.) If our tropical circulation is steady, we expect that it will always be raining and convecting in the intertropical convergence zone, so that $\hat{\Theta}_0=\hat{\Theta}_{\text{crit}}$, and the Hadley cell will transport energy out of the ITCZ only if

$$Lr_0<2c_pA\hat{\Theta}_{\text{crit}}.$$

We guarantee that this inequality will be satisfied by defining $r_{\max}(\bar{T})\equiv\alpha r_s$, where

$$r_s\equiv 2c_pA\hat{\Theta}_{\text{crit}}(\bar{T})/L \quad (4)$$

and where α is a constant smaller than unity, and then requiring that $r\leqslant r_{\max}$. We refer to r_s as the saturation mixing ratio and to α as the precipitation criterion. [We could equally well have defined r_s first, as the saturation mixing ratio at 750 mb obtained from the Clausius–Clapyron equation, for example, and then have used (4) to define $\hat{\Theta}_{\text{crit}}$.]

Statistically steady states of models with different values of α are compared in Section 6. On the basis of this comparison, we choose the value $\alpha=0.8$ for our "moist" integrations. As discussed in Section 6, we have some hope that the arbitrariness involved in the choice of α does not have serious consequences for the model's climatic responses.

In order to convectively adjust and precipitate, we first transform the potential temperature and moisture fields onto grid points in the zonal direction. If $r<r_{\max}$

at a grid point, no precipitation or adjustment occurs. If $r>r_{\max}$, an amount of water

$$\delta r=(r-r_{\max})\Big/\left[1+\left(\frac{L}{2c_p}\right)\frac{dr_{\max}}{d\bar{T}}\right]$$

is precipitated and the latent heat $L\delta r$ released in the lower layer. If $\hat{\Theta}<\hat{\Theta}_{\text{crit}}$ after this heat release, $\hat{\Theta}$ is set equal to $\hat{\Theta}_{\text{crit}}$, $\bar{\Theta}$ being adjusted simultaneously to conserve $\bar{T}$. After the precipitation and adjustment, all fields are returned to zonal wavenumber space, discarding those wavenumbers produced by these processes but not included in the spectral truncation.

c. Surface fluxes

The surface is assumed to have zero heat capacity, so that

$$S=H+LE.$$

S is the net downward radiative flux at the surface, and H and E are the upward sensible heat flux and evaporation. Zonal asymmetries in the surface energy balance are ignored; H, E and S are independent of longitude.

S is obtained from the radiative parameterization described above. The following relations are used to compute H and E:

$$\left.\begin{aligned}H&=-C(T_s-T_*)=\left(\frac{\Delta p}{g}\right)Q_0^{\text{sh}}\\E&=-C[h_sR(T_s)-h_*R(T_*)]=\left(\frac{\Delta p}{g}\right)W_0^{\text{evap}}\end{aligned}\right\},\qquad(5)$$

where $R(T)$ is the saturation mixing ratio at 1000 mb obtained from the Clausius–Clapyron equation. The relative humidity in the atmosphere at the ground, h_s, is assumed, somewhat arbitrarily, to be given by $1-h_s\equiv 0.5(1-h_0)$, where $h_0\equiv r_0/r_s$ and r_0 is the predicted zonally averaged mixing ratio in the lower layer. h_* is simply set equal to 1; the surface is assumed to be everywhere saturated (the "swamp" lower boundary condition utilized by Manabe).

The coefficient C depends on the magnitude of the zonally averaged wind in the lower layer

$$C=(1.1\times10^{-3})\rho_s\max(|u_{2,0}|,\ 5\text{ m s}^{-1}),\qquad(6)$$

where $\rho_s\equiv 1.25\times10^{-3}$ g cm^{-3}. The lower limit on C avoids an unrealistic surface energy balance when $|u_{2,0}|$ is small. (Having imposed this lower limit, we use $|u_{2,0}|$ in the definition (6) rather than $|u_{2,0}^2+v_{2,0}^2|^{\frac{1}{2}}$, the speed of the lower layer zonal wind, since $v_{2,0}\lesssim 1$ m s^{-1}).

The momentum transfer from the surface to the lower layer of the atmosphere in both zonal and eddy equations is also given by a drag law,

$$\mathbf{F}^{\text{surf}}=-C\mathbf{v}_2\frac{g}{\Delta p}.$$

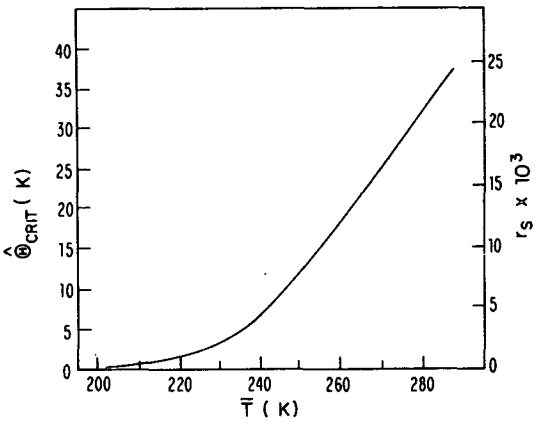

FIG. 3. The static stability $\hat{\Theta}=[\Theta(250\text{ mb})-\Theta(750\text{ mb})]/2$ of an atmosphere with a moist adiabatic temperature profile, as a function of the mean temperature

$$\bar{T}=[T(250\text{ mb})+T(750\text{ mb})]/2.$$

d. Horizontal diffusion

No attempt is made to justify the procedure used for subgrid-scale mixing on any fundamental grounds.

Linear diffusion is used in the eddy ($m\neq 0$) momentum, potential temperature and moisture equations, with a diffusion coefficient D equal to 3.5×10^5 m^2 s^{-1}. Smaller values of D allow more eddy kinetic energy to develop but lead to unreasonable amounts of noise in the solutions. (An example of a "reasonable" amount of noise is displayed below.)

Linear diffusion in the zonally averaged equations with this value of D would result in substantial time-averaged diffusive fluxes. We therefore use a non-linear diffusion in the $m=0$ equations of the form proposed by Smagorinsky (1963), in which the diffusion constant is taken to be proportional to the magnitude of the local rate of deformation of the flow

$$D_k=D_*\frac{\cos(\theta)}{a}\left\{\left[\frac{\partial}{\partial\theta}\left(\frac{u_{k,0}}{\cos(\theta)}\right)\right]^2+\left[\frac{\partial}{\partial\theta}\left(\frac{v_{k,0}}{\cos(\theta)}\right)\right]^2\right\}^{\frac{1}{2}}.$$

We choose the constant of proportionality D_* to be $0.003\ \Delta^2/\cos(\theta)$ where Δ is the meridional grid spacing. The $\cos(\theta)^{-1}$ weighting factor is used simply because mixing is found to be particularly helpful in controlling occasional severe noise near the polar boundaries. Typically, 70% of the model's dissipation of eddy kinetic energy and only 10% of its dissipation of zonal kinetic energy occur through lateral diffusion, the rest of the energy being lost through surface drag. (We recognize the large diffusive eddy kinetic energy loss as a model weakness.)

In order to give the reader some idea of the character of the time evolution predicted by a model of this sort, we display in Fig. 4 a contour plot of the zonally and

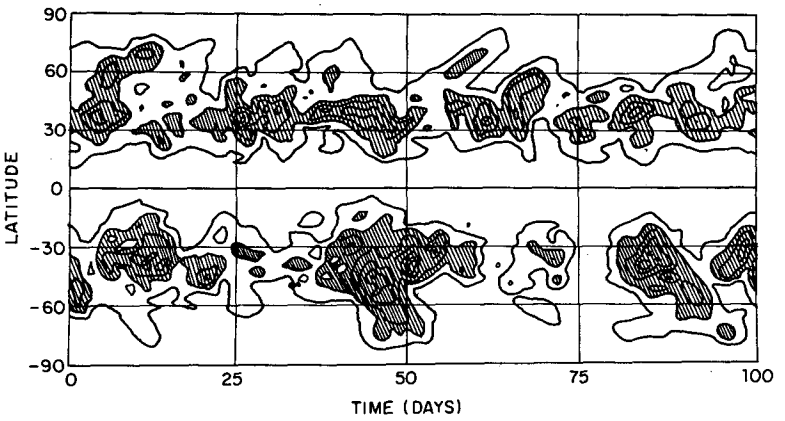

FIG. 4. Time evolution of the vertically and zonally averaged eddy kinetic energy predicted by the 2-wave $m=3$, 6 moist model during a 100-day period after attaining a statistically steady state. The contouring interval is 25 $m^2 s^{-2}$. Regions corresponding to energies greater than 50 $m^2 s^{-2}$ are hatched.

vertically averaged eddy kinetic energy,

$$\sum_m \overline{|\mathbf{v}_m|^2}(\theta,t),$$

produced by the two-wave, $m=3$, 6 moist model (discussed in Section 5) after it has reached its statistically steady state. Contours are obtained by linearly interpolating between daily averages. The eddies are seen to have large variability on time scales of 20 to 50 days with no apparent periodicities. Although confined primarily to mid-latitudes, they do cause considerable variability in polar as well as midlatitude temperatures and zonal winds.

The evolution in this 100-day period of the globally averaged eddy kinetic energy balance is shown in Fig. 5. The conversions from potential and zonal kinetic into eddy kinetic energy and the dissipation of eddy kinetic energy by lateral diffusion and surface drag are plotted as functions of time. [The definitions of the conversions are standard and can be found, for example, in Lorenz (1960).] The model produces much greater variability in the conversions from potential and zonal kinetic into eddy kinetic energy than in the dissipative terms—eddies decay not because the rate of dissipation becomes extraordinarily large, but because the rate of energy generation drops below the relative steady rate of dissipation. We also note that the conversion of eddy kinetic into zonal kinetic energy seems to play a significant role in the finite-amplitude dynamics of the eddies, even though the time average of this conversion is quite small.

3. The dry model

Results from this "moist" model are not easily compared with theories for eddy fluxes, such as that

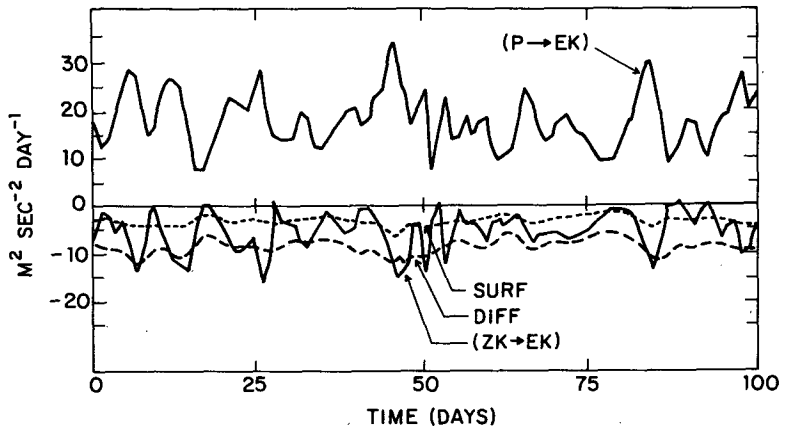

FIG. 5. Evolution of the globally averaged eddy kinetic energy balance for the same time period as in Fig. 4. (P → EK) is the conversion from potential into eddy kinetic energy, (ZK → EK) the conversion from zonal kinetic into eddy kinetic energy, (SURF) the rate of dissipation of eddy kinetic energy by surface drag, and (DIFF) the rate of dissipation of eddy kinetic energy by lateral diffusion.

of Stone (1972), that are meant to apply to an atmosphere in which the static stability is maintained by large scale vertical sensible heat fluxes rather than by moist convection. We examine a dry version of the model from which the moist convective adjustment has been removed in order to facilitate such comparisons and in order to examine the importance of the character of the static stability balance for climatic sensitivity.

We do not remove all of the effects of water from the model, as this would create drastic changes in the radiative fluxes, making comparisons with the moist results difficult. The radiative effects of water vapor and clouds are computed exactly as in the moist model, as is the evaporation from the surface [with h_s in Eq. (5) set equal to 0.8], but evaporated water is immediately condensed, releasing latent heat in the lower layer. The atmosphere no longer transports water vapor.

Just as we choose a value of the precipitation criterion in the moist model to produce a steady Hadley cell, in the dry model we choose a minimum value of $\hat{\Theta}$, $\hat{\Theta}_{\min}>0$, to be maintained by a dry convective adjustment. The imposition of a minimum stability can also be thought of as an artificial constraint preventing the local radius of deformation from becoming smaller than the grid size, at which point the model will have difficulty in simulating geostrophic adjustment (Arakawa and Lamb, 1977). The value $\hat{\Theta}_{\min}=2.5$°C is found to provide a suitably steady low-latitude circulation and is used in all of our dry integrations.

4. Statistical analysis

Our estimates of the statistically steady states (or climates) of this atmospheric model will, of course, be based on time integrations of finite length and will, therefore, be uncertain. Estimates of this uncertainty are essential for determining the significance of climatic responses to perturbations in external parameters.

The problem is to determine the variance $\mu_T(\rho)$ in the statistically steady state of averages of length T of some variable ρ of interest. As discussed by Leith (1973), this variance is given by

$$\frac{\mu_T}{\mu}\equiv\frac{2}{T}\int_0^T \mathcal{R}(\tau)(1-\tau/T)d\tau,$$

where

$$\mathcal{R}(\tau)\equiv\{\rho'(0)\rho'(\tau)\}/\mu,$$
$$\rho'\equiv\rho-\{\rho\},$$
$$\mu\equiv\{\rho'^2\},$$

and where brackets denote a time average. Given one integration of length T, one can only evaluate $\mu_{T'}(\rho)$ for some $T'\ll T$ and then try to extrapolate from $\mu_{T'}(\rho)$ to $\mu_T(\rho)$.

For a red noise spectrum, the lagged autocorrelation function is a decaying exponential $\mathcal{R}(\tau)=e^{-\tau/\tau_0}$ and

$$\frac{\mu_T^{\text{red noise}}}{\mu}\equiv\mathfrak{N}_T(\tau_0)\equiv\frac{2\tau_0}{T}\left\{1-(1-e^{-T/\tau_0})\frac{\tau_0}{T}\right\}.$$

We calculate an effective correlation decay time τ_0 for the variable ρ by solving the equation

$$\mathfrak{N}_{T'}(\tau_0)=\mu_{T'}/\mu$$

for τ_0 and then assume that the ratio of $\mu_{T'}$ to μ_T is approximately that of a red noise spectrum with this value of τ_0, i.e.,

$$\frac{\mu_T}{\mu}\approx\mathfrak{N}_T(\tau_0).$$

Estimates of the standard deviations of averages of length T—$(\mu_T)^{\frac{1}{2}}$—where T is either 200 or 400 days, will

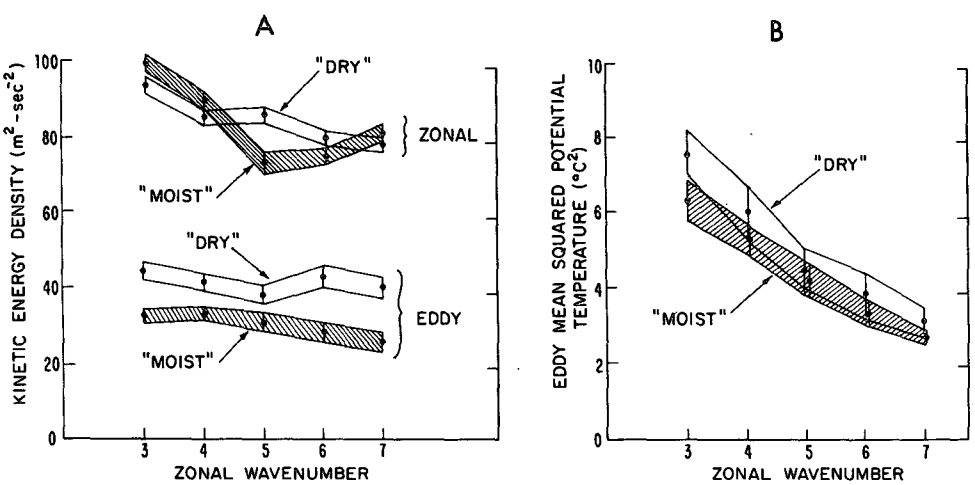

FIG. 6. Globally averaged zonal and eddy kinetic energies (a) and variances of eddy potential temperature (b) produced by moist and dry 1-wave models with $m=3$, 4, 5, 6 and 7. The dots are 200-day averages. The vertical error bars have length $2\mu^{\frac{1}{2}}$, where μ is the estimated variance of 200-day averages.

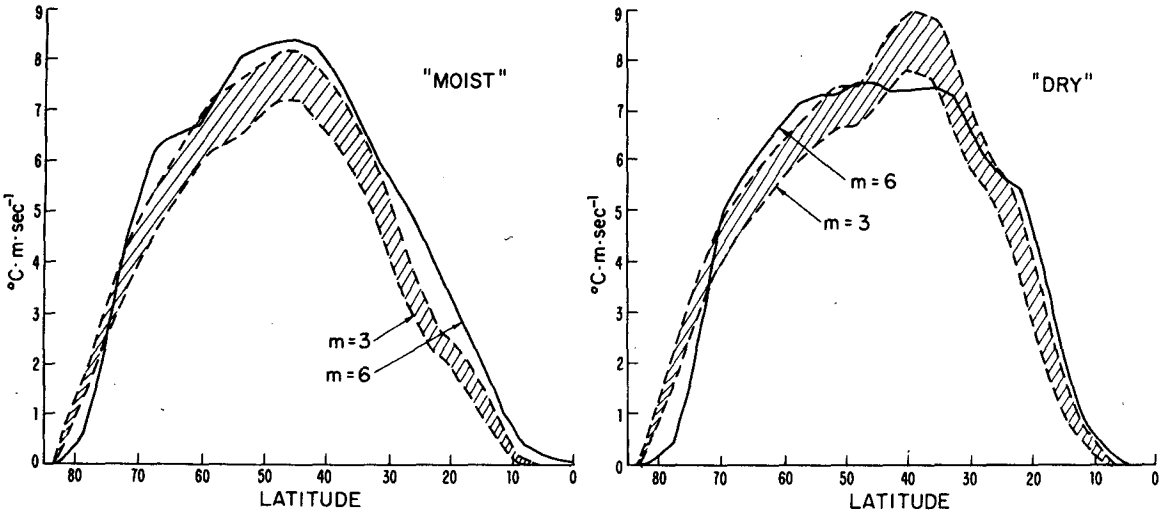

FIG. 7. The vertically averaged poleward flux of potential temperature, $2\,\mathrm{Re}(\overline{v_m\Theta_m^*})$, in the moist and dry 1-wave models with $m=3$ and $m=6$. For $m=3$, we plot the 200-day time average $\pm$ the estimated standard deviation of 200-day time averages.

be included in many of the figures describing properties of the model's statistically steady states without further comment in the text. These estimates depend to some extent on the choice of T'. We have simply chosen $T'=T/20$ in every case.

All of our integrations begin from an isothermal state of rest plus a small random perturbation in the eddy temperatures. We begin gathering statistics for the analysis described above after 300 model days, by which time features of the model with little variability, such as the global mean temperature, seem to have reached their steady values.

Since the model is on a sphere but forced with radiation symmetric about the equator, we make use of the duplicate information by calculating $\{\rho\}$ and $\mu_T(\rho)$ separately in each hemisphere and averaging the results.

5. Spectral truncation

a. One-wave experiments

We begin the discussion of the statistically steady states produced by this model by examining a variety of experiments in which only the zonally averaged flow and one nonzero zonal wavenumber are retained. All of the experiments are of 500 days duration. Climatic statistics are obtained from the final 200 days of integration.

In Fig. 6a the globally averaged zonal and eddy kinetic energies are plotted for ten such experiments, with $m=3$, 4, 5, 6 and 7 in the moist and dry models. We note that the moist models have less eddy kinetic energy than their dry counterparts—a plausible result, since a most eddy, carrying latent as well as sensible heat poleward, has a larger effect on the mean temperature gradient than a dry eddy of the same size, and can therefore be expected to equilibrate at a smaller amplitude. We note also that all of the models develop considerably less eddy kinetic energy than does the earth's atmosphere, where the ratio of zonal to eddy kinetic energy is less than unity (Oort and Peixoto, 1974). In trying to select the best one-wave model, one might consider selecting that wavenumber which produces the most energetic eddies. No such wavenumber stands out clearly in the comparison of eddy kinetic energies in Fig. 6a. The different wavenumbers do, however, differ significantly in the variances of eddy potential temperature they maintain. The global average of $2\overline{|\Theta_m|^2}$ for each of these one-wave experiments is plotted in Fig. 6b.

Of primary interest for climatic sensitivity experiments, however, is the model's poleward flux of potential temperature. In Fig. 7 we show $2\,\mathrm{Re}\,(\overline{v_m\Theta_m^*})$ as a function of latitude for the $m=3$ and $m=6$ moist and dry models. In both moist and dry cases, the $m=6$ transport out of the tropics and subtropics is greater than the $m=3$ transport. The $m=6$ transport also dies out more rapidly as it nears the polar boundary. Yet it is the rough similarity between the $m=3$ and $m=6$ fluxes that is most intriguing, in light of the large differences in temperature variance—this being our first indication that the distortion of eddy structure due to severe spectral truncation may not be a particularly serious source of error.

Also of considerable interest for climatic sensitivity studies, however, is the vertical flux of potential temperature, $-2\,\mathrm{Re}(\omega_m\bar{\Theta}_m^*)$, plotted in Fig. 8 for these same experiments. Whereas the $m=3$ models have one maximum in the vertical flux in mid-latitudes, the $m=6$ models have a secondary maximum in subpolar

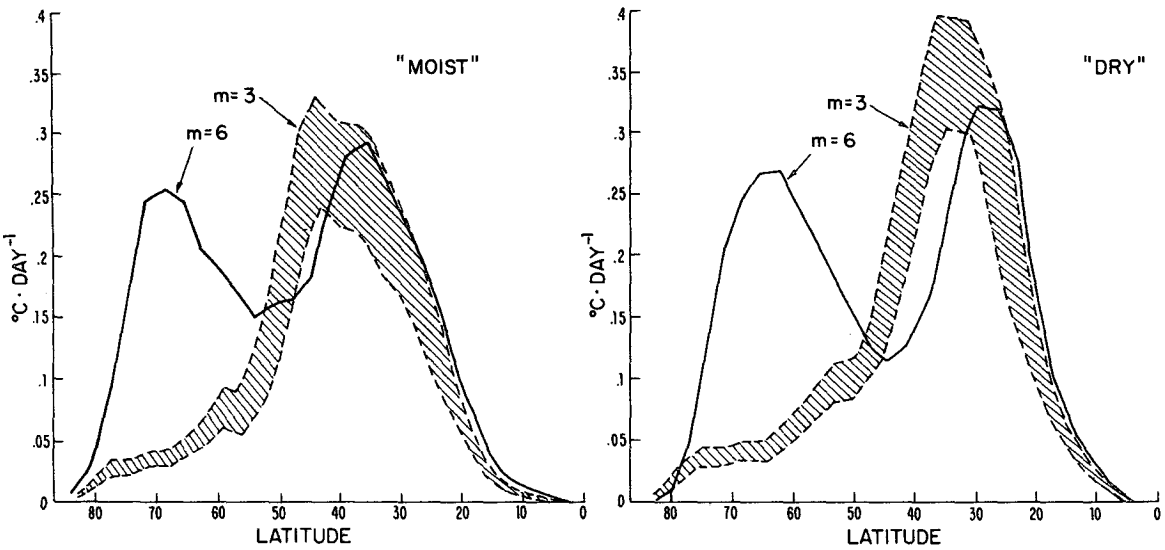

FIG. 8. The vertical flux of potential temperature across 500 mb (divided by $\Delta p \cong 500$ mb), $-2\,\mathrm{Re}(\omega_m \bar{\Theta}_m^*)$, in the "moist" and dry 1-wave models with $m=3$ and $m=6$. Estimated standard deviations for 200-day averages are again shown for $m=3$.

latitudes. Analogous plots for a multi-level general circulation model [Fig. 7-2 in Manabe, *et al.* (1974)] show no such secondary maximum. (Comparison cannot be made with observations on this point since the transient vertical eddy flux cannot be computed from available data.)

The zonally averaged mean atmospheric potential temperatures $\bar{\Theta}_0$ and static stabilities $\hat{\Theta}_0$ maintained in these experiments are displayed in Fig. 9. We include for comparison plots of the potential temperatures in moist and dry radiative-convective equilibria, obtained by forcing the thermodynamic equations of the model

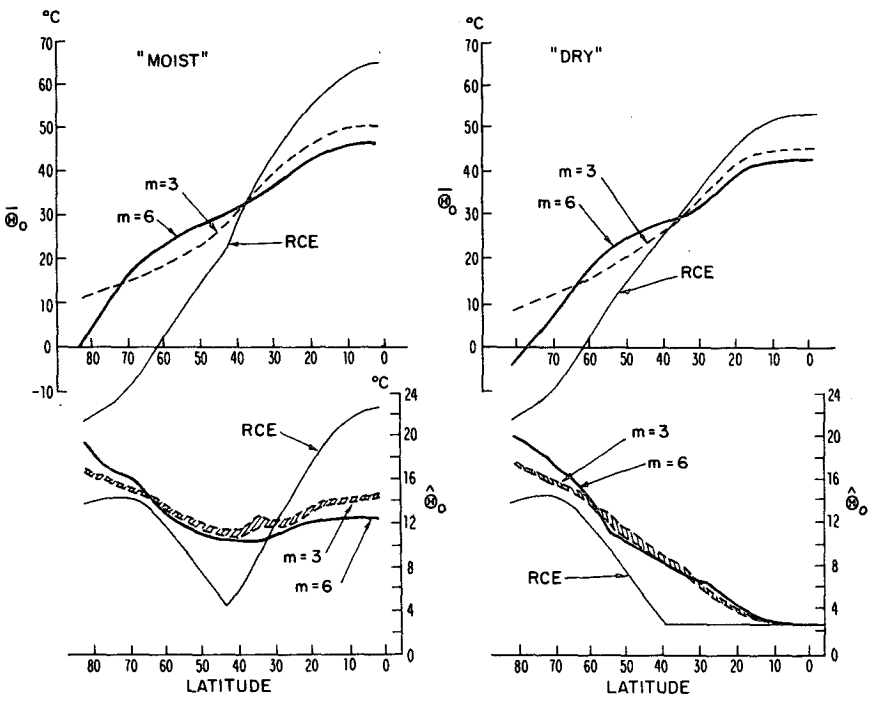

FIG. 9. Vertically averaged potential temperature $\bar{\Theta}_0$ and static stability $\hat{\Theta}_0$ in the $m=3$ and $m=6$ 1-wave models, compared with moist and dry radiative-convective equilibria (RCE). Estimated standard deviations of 200-day averages are shown for $\hat{\Theta}_0$ with $m=3$. Estimated standard deviations for $\bar{\Theta}_0$ are $\sim$0.2°C.

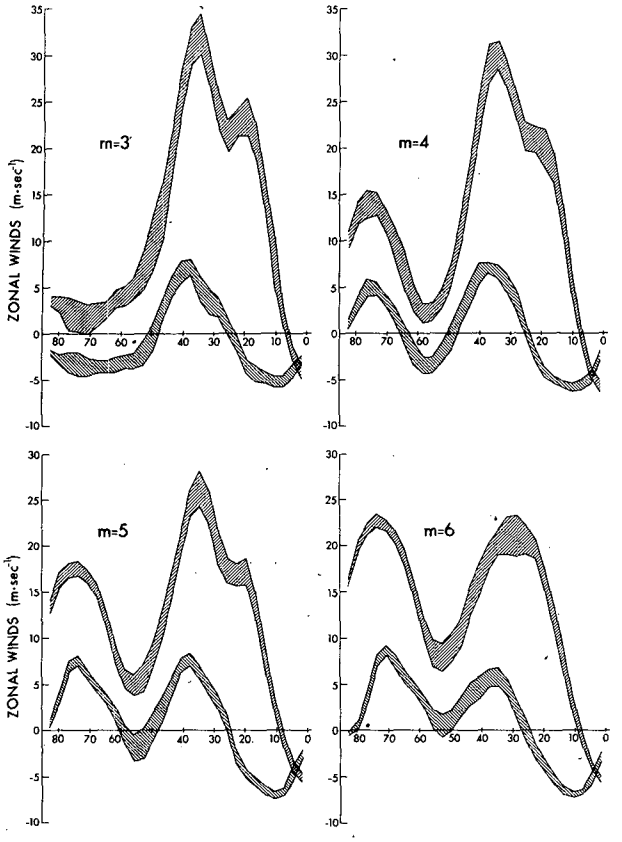

FIG. 10. Upper and lower layer zonal winds produced by moist and dry 1-wave models with $m=3$, 4, 5 and 6. Estimated standard deviations of 200-day averages are shown in each case.

with radiative fluxes, boundary fluxes and a convective adjustment and integrating in time until a steady state is achieved. [In the moist radiative-convective calculation, the atmosphere is assumed to be saturated, so that $\hat{\Theta} \gtrsim \hat{\Theta}_{\text{crit}}(\bar{T})$.] In both moist and dry models, $m=6$ is cooler than $m=3$ near the pole (although still considerably warmer than radiative equilibrium), warmer in the latitude span 40–70°, and cooler once again in the tropics, consistent with the horizontal fluxes in Fig. 7. Differences in $\bar{\Theta}_0$ are substantial ($\gtrsim 5$°C) in high latitudes, differences in temperature gradients being even more significant. Differences in $\hat{\Theta}_0$, on the other hand, are relatively small despite the large changes in the vertical eddy flux in high latitudes. As a result, changes in the atmospheric temperature at the ground ($T_s = 0.986\bar{\Theta}_0 - 1.337\hat{\Theta}_0$) are predominantly due to changes in $\bar{\Theta}_0$. Whereas $\bar{\Theta}_0$ in high latitudes is maintained above its radiative equilibrium value almost exclusively by the horizontal eddy flux of potential temperature, the role of the vertical eddy fluxes in maintaining the static stability is less clear cut. The difference in the high latitude vertical flux between the $m=3$ and $m=6$ experiments is, in fact, almost balanced by changes in the contributions of the meridional circulation and the horizontal fluxes to $\partial\hat{\Theta}_0/\partial t$, so that the total dynamical contribution changes very little. We take a closer look at the model's stability balance in Section 7.

In Fig. 10 we compare the zonal winds produced by the 1-wave moist models with $m=3$, 4, 5 and 6. The winds in the dry model behave in an entirely similar manner and are not shown. Wavenumber 6 maintains a well-defined two-jet structure in the zonal wind, with a subpolar jet of about the same strength as the subtropical jet. Beneath both the upper level subpolar and subtropical jets there are strong lower level (or surface) westerlies. As m is reduced, the strength of the subtropical jet increases somewhat and that of the subpolar jet decreases. With $m=3$, no trace of the subpolar jet remains and the low-level winds in high latitudes have become easterlies. The boundary between low-level easterlies and westerlies in the subtropics, however, is insensitive to the choice of zonal wavenumber.

We suggest the following explanation for this behavior of the high latitude zonal winds. If we approximate our equations with a quasi-geostrophic model with fixed static stability on a β-plane at latitude θ and consider Phillip's (1951) stability analysis of a zonal flow with constant vertical shear and no horizontal shear, we find that all unstable waves must have zonal wavenumber $m < m_*$, where

$$m_* \equiv 2\Omega a \sin(\theta)\cos(\theta)/(c_p B\hat{\Theta}_0)^{\frac{1}{2}}$$
$$\approx 84 \sin(\theta)\cos(\theta)/\hat{\Theta}_0{}^{\frac{1}{2}}.$$

(The second formula holds if $\hat{\Theta}_0$ is expressed in °C.) Because of the convergence of meridians [the $\cos(\theta)$ factor in m_*] $m=6$ is too small to be strongly baroclinically unstable poleward of ~ 70°. As a result, in the $m=6$ experiment heat is transported into high latitudes very inefficiently and large temperature gradients develop poleward of where most of this heat is deposited. Since quasi-geostrophic waves transport net westerly momentum into regions of large vertical shear (see, e.g., Held, 1975), low-level westerlies must develop to provide the surface drag to balance these momentum fluxes. Although somewhat less efficient in transporting heat out of the subtropics, $m=3$ is considerably better at transporting heat into polar latitudes.

Figs. 11 and 12 illustrate how the upper and lower level winds are maintained in the $m=3$ and $m=6$ experiments. In the upper layer

$$\frac{\partial u_{1,0}}{\partial t} = \underbrace{-\frac{1}{a\cos^2(\theta)}\frac{\partial}{\partial\theta}[\cos^2(\theta)u_{1,0}v_{1,0}] - \omega_0\bar{u}_0}_{\text{MMC}}$$
$$\underbrace{-\frac{1}{a\cos^2(\theta)}\frac{\partial}{\partial\theta}[\cos^2(\theta)2\,\text{Re}(u_{1,m}v^*_{1,m})]}_{\text{Horizontal eddies}}$$
$$\underbrace{-2\,\text{Re}(\omega_m\bar{u}^*_m)}_{\text{Vertical eddies}} + \underbrace{f\bar{v}_0}_{\text{Coriolis}} + \underbrace{F^{\text{diff},\lambda}_{1,0}}_{\text{Diffusion}}.$$

In the lower layer

$$\frac{\partial u_{2,0}}{\partial t} = \underbrace{-\frac{1}{a\cos^2(\theta)}\frac{\partial}{\partial\theta}[\cos^2(\theta)u_{2,0}v_{2,0}]+\omega_0\bar{u}_0}_{\text{MMC}}$$

$$\underbrace{-\frac{1}{a\cos^2(\theta)}\frac{\partial}{\partial\theta}[\cos^2(\theta)2\,\mathrm{Re}(u_{2,m}v^*_{2,m})]}_{\text{Horizontal eddies}}$$

$$+\underbrace{2\,\mathrm{Re}(\omega_m\bar{u}^*_m)}_{\text{Vertical eddies}}-\underbrace{f\bar{v}_0}_{\text{Coriolis}}-\underbrace{Cu_{2,0}}_{\text{Surface drag}}+\underbrace{F^{\text{diff},\lambda}_{2,0}}_{\text{Diffusion}}.$$

The nomenclature beneath the various terms is that used in the figures. The contribution of diffusion to the rate of change of zonal winds has not been plotted, as it is everywhere less than 0.15 m s^{-1} day^{-1}.

The Coriolis torque in the lower layer is primarily balanced by surface drag (except in high latitudes in the $m=6$ experiment, where the eddy flux convergence is also important) and one can generally obtain the sign of the meridional circulation from that of the lower layer zonal wind. In the upper layer, the dominant balance is that between the horizontal momentum flux convergence and the Coriolis force. In the $m=6$ case there are, therefore, two strong indirect cells corresponding to the two maxima in horizontal flux convergence and the two regions of strong surface westerlies. In the $m=3$ experiment, there is one indirect cell associated with the momentum flux convergence in midlatitudes, surrounded by direct Hadley and polar cells—the classic three-cell pattern.

Evidently, a low wavenumber capable of efficiently transporting heat into polar latitudes is required by this model if it is to produce a moderately realistic climate in high latitudes. We have therefore chosen the 1-wave $m=3$ model for comparison with the multiwave models in the following section.

b. *Multiwave experiments*

In order to select those waves most likely to modify the circulation produced by $m=3$, we again refer to the stability analysis for a quasi-geostrophic 2-level model on a β-plane. We take the values of $\hat{u}_0$ and $\hat{\Theta}_0$ produced by the $m=3$ moist and dry models, and the values of f and β at each latitude, and compute the growth rate as a function of zonal wavenumber k and meridional wavenumber l

$$\omega_I \equiv k(4\hat{u}_0{}^2K^4(F^2-K^4)-\beta^2F^2)^{\frac{1}{2}}/2K^2(K^2+F), \quad (7)$$

where

$$F\equiv f^2/c_pB\hat{\Theta}_0, \quad k\equiv m/a\cos(\theta), \quad K^2\equiv k^2+l^2.$$

For a given m, we find that value of l which maximizes ω_I and plot the resulting growth rates in Fig. 13.

The linear instability of some simple baroclinic flows in a two-level balanced model on a sphere has been

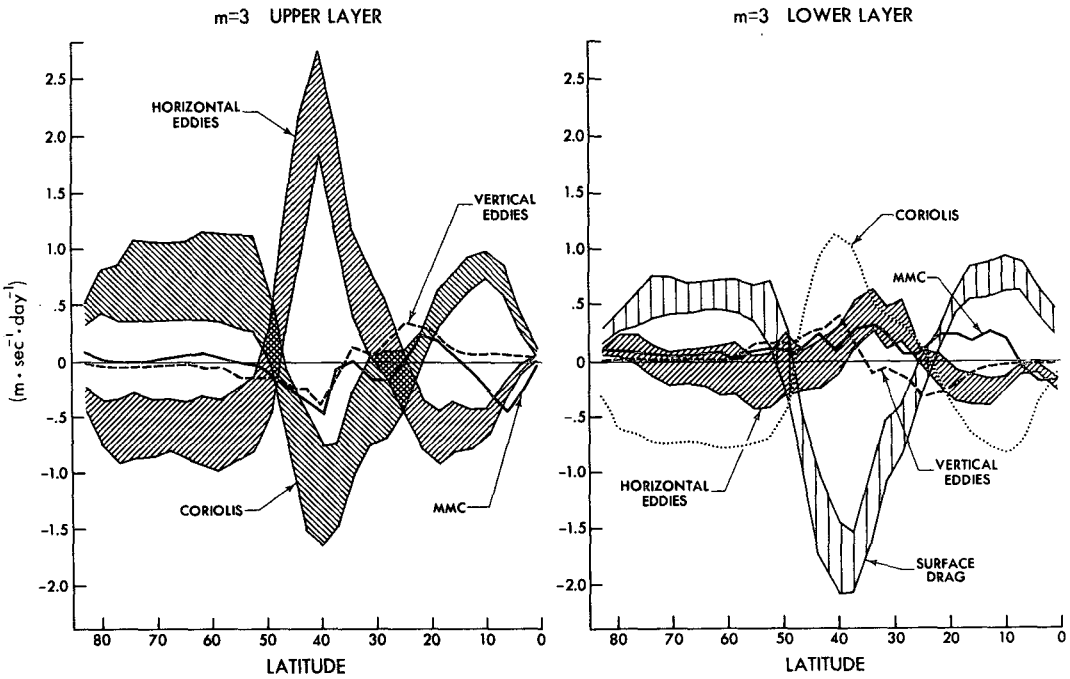

FIG. 11. The maintenance of the upper and lower layer zonal winds in the $m=3$ moist experiment. For selected terms—the horizontal eddy flux convergence and surface drag in the lower layer, and the horizontal flux convergence and Coriolis force in the upper layer—we plot time averages $\pm$ estimated standard deviations of 200-day averages. Definitions of the various terms are given in the text.

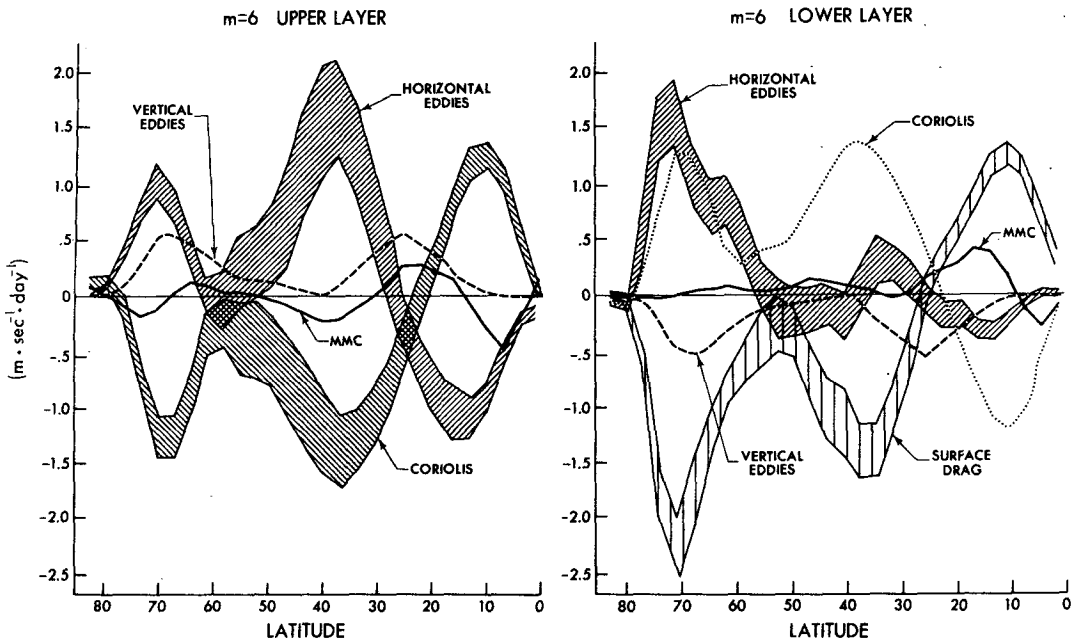

FIG. 12. The maintenance of the upper and lower layer zonal winds in the $m=6$ moist experiment.

investigated by Moura and Stone (1976). Their analysis confirms the intuitive notion that the most unstable wave has maximum amplitude at approximately that latitude where the flow is most unstable locally and that its wavelength is roughly determined by the local stability analysis at that latitude. We therefore interpret Fig. 13 as implying that the zonal circulation maintained by $m=3$ in both moist and dry models will be strongly unstable to shorter waves, maximum instability occurring at $\sim 40°$ in the moist case and at $\sim 30°$ in the dry case.

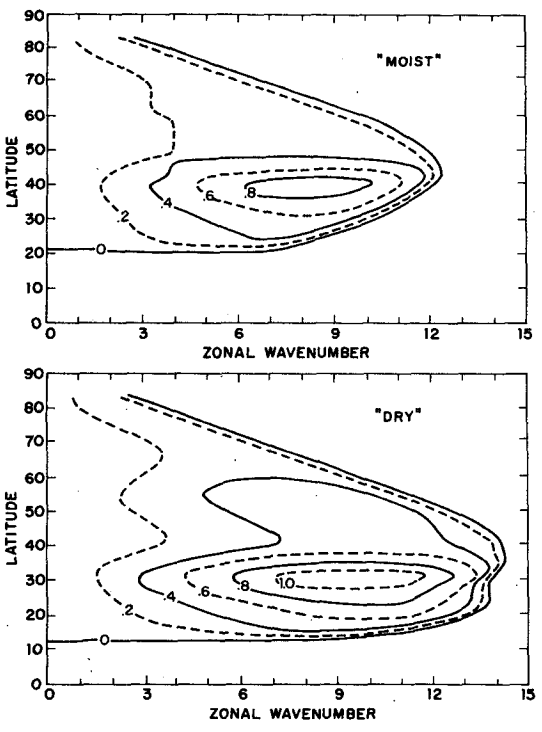

FIG. 13. The growth rate ω_I (day^{-1}) as a function of latitude and zonal wavenumber, obtained from (7) using the values of $\hat{u}_0$ and $\hat{\Theta}_0$ produced by the 1-wave $m=3$ moist and dry models.

We compare the 1-wave $m=3$ model with 2-wave, $m=3$, 6 and 3-wave $m=3$, 6, 9 models to see how the circulation changes when these smaller waves are added. The experiments are each of 700 days duration, the period of time-averaging being the final 400 days of integration. Identical experiments have been performed with the moist and dry models. The effect of different spectral truncations on the dry results is very similar to their effect on the moist results, and we describe the circulations in the moist cases only.

Fig. 14 shows the time averages of $\overline{|\mathbf{v}_m|^2}$, $2\,\mathrm{Re}(\overline{v_m\Theta_m^*})\times\cos(\theta)$, and $-2\,\mathrm{Re}(\omega_m\overline{\Theta_m^*})$ for each of the waves in the three experiments. We see that the kinetic energy is rather evenly apportioned among the available waves, and that the total eddy kinetic energy and its distribution as a function of latitude are very similar in the three experiments. The horizontal flux of potential temperature increases about 20% in midlatitudes when $m=6$ is added to $m=3$, and the vertical flux increases about 30%. Neither the horizontal nor the vertical flux change significantly when $m=9$ is included, despite the fact that $m=9$ is then responsible for a considerable fraction of these fluxes. We note also that the partitioning of the poleward heat flux between the various waves is strongly latitude dependent, with $m=3$

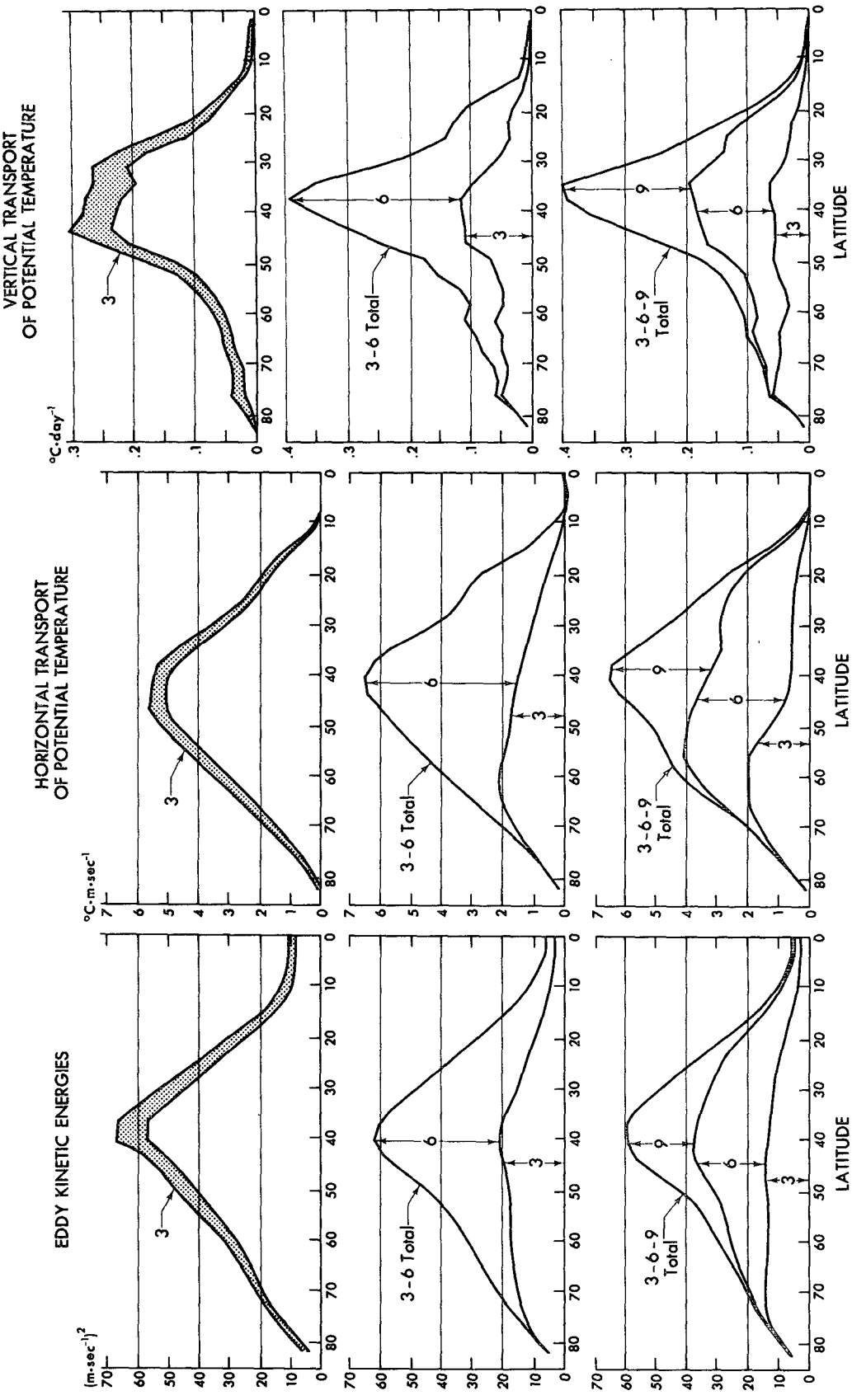

FIG. 14. Vertically averaged eddy kinetic energy, vertically averaged horizontal eddy flux of potential temperature, and vertical eddy flux of potential temperature, in the 1-, 2-, and 3-wave experiments. Estimated standard deviations are shown for the 1-wave experiment. Note that ω has been divided by Δp, so that the vertical flux has the units of a heating rate.

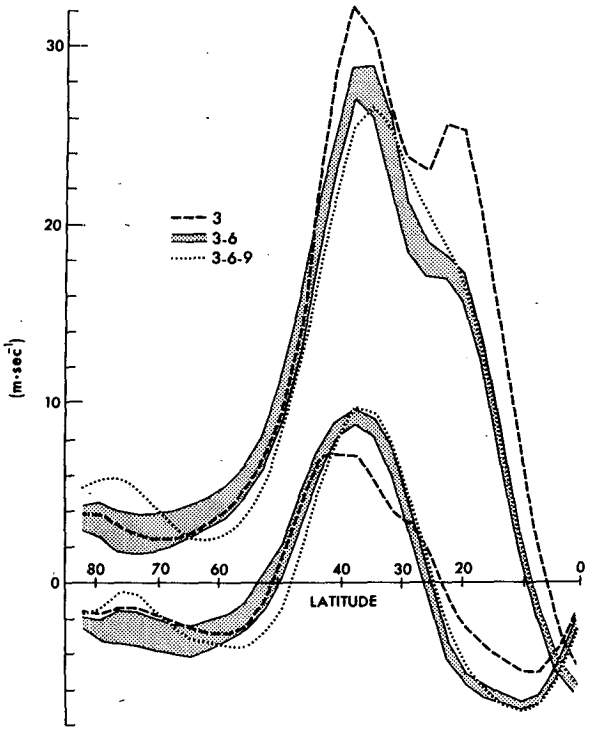

FIG. 15. Upper and lower layer zonal winds in the 1-, 2-, and 3-wave experiments. Estimated standard deviations are shown for the 2-wave experiment.

retaining its importance for heat transport into high latitudes.

When $m=6$ is added to $m=3$, tropical temperatures and subtropical temperature gradients decrease and polar temperatures increase slightly, the pole-to-equator temperature difference decreasing $\sim 6°C$—the sort of behavior expected from a model combining the attributes of the $m=3$ and $m=6$ 1-wave models. When $m=9$ is added to 3 and 6, subtropical gradients again decrease very slightly and tropical temperatures drop $\sim 1°C$. The static stabilities, once again, are very similar in the various experiments.

In Fig. 15 we plot the upper and lower layer zonal winds in these experiments. When the shorter waves are added to $m=3$, surface winds in low and middle latitudes increase, as the shorter waves are carrying somewhat more momentum as well as heat. These stronger low-level winds in the multiwave cases are consistent with the stronger meridional circulations shown in Fig. 16, the momentum balance in the multiwave experiments being very similar to that in the $m=3$ experiment discussed earlier. Changes in circulation that occur when $m=6$ is added to $m=3$ are considerably greater than changes that occur when $m=9$ is added to 6 and 3.

The multiwave models also transport more water vapor out of the subtropics, as demonstrated in Fig. 17, a plot of time-averaged precipitation. The 2-wave and 3-wave models produce a secondary maximum in precipitation at 37.5°, while $m=3$ alone produces a weaker maximum at 25.5°. The intertropical convergence zone, centered at the equator in all of our experiments, is also somewhat weaker in the one-wave model, due to the weaker meridional circulation. The precipitation patterns produced by the 2- and 3-wave models, on the other hand, are remarkably similar both in mid-latitudes and in the tropics.

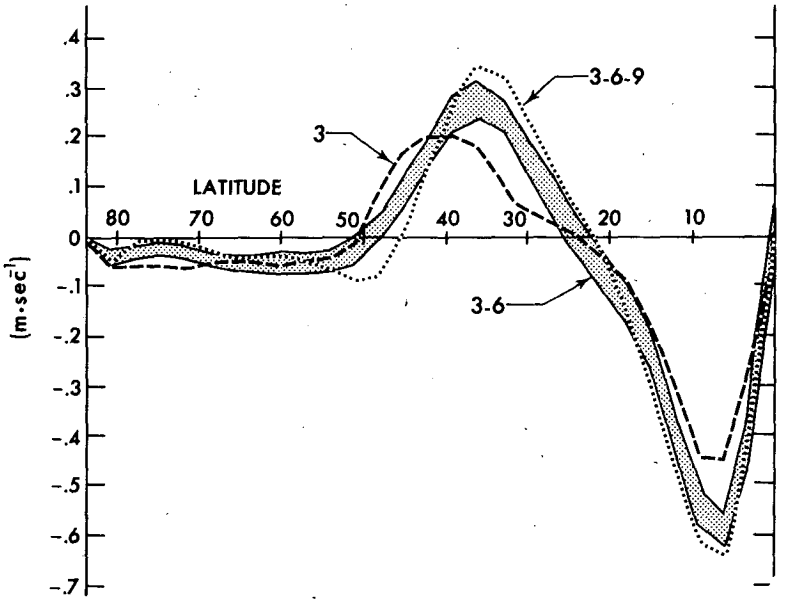

FIG. 16. The mean meridional circulation $\hat{v}_0$ in the 1- 2- and 3-wave experiments. Negative values of $\hat{v}_0$ correspond to a direct circulation (poleward flow aloft).

It is surprising, in light of Fig. 13, that $m=9$ does not have a much more substantial impact of the time-averaged flow in mid-latitudes and in the subtropics. Local stability plots for the time-averaged flows produced by the 2- and 3-wave models are very similar to those in Fig. 13. For example, growth rates in the region of strong instability at 40° in the "moist" case are only ~20% smaller for the flow produced in the $m=3$, 6 model than for the flow produced by $m=3$ alone. Further changes when $m=9$ is introduced are even smaller. Yet the local stability analysis seems to have validity since $m=9$ develops substantial amplitude at just that latitude predicted by the analysis. It seems, therefore, that exclusion from the model of waves that are strongly unstable on the time-averaged zonal flow (such as the still smaller waves which Fig. 13 suggests would develop in the subtropics of the dry model) is not necessarily a serious limitation.

It is also surprising that $m=3$, which contributes so little to the midlatitude horizontal and vertical eddy fluxes when forced to compete with $m=6$ and 9, is yet capable of maintaining fluxes of more or less the correct magnitude when acting alone. Such results suggest that adequate theories for these eddy fluxes may exist which do not depend on detailed knowledge of eddy structure.

Considering the rather gross climatic sensitivity experiments contemplated for this model, the differences between the circulations produced by the 3-6 and the 3-6-9 models are too small to warrant the additional computational burden in the 3-wave model. On the other hand, we find the decrease of 6°C in pole-to-equator temperature difference and the changes in the precipitation pattern to be significant enough to recommend the use of the two-wave over the one-wave model. We have therefore chosen the 3-6 model in both its moist and dry versions for further study.

The peculiar behavior exhibited in high latitudes by the 1-wave models with $m>3$ warns us of an important limitation of the 3-6 model. If we perturb the system so that $\hat{\Theta}_0$ is high latitudes increases substantially (or if the rotation rate Ω decreases) the shortwave cutoff, m_*, will decrease, $m=3$ will no longer be able to transport heat as efficiently into high latitudes, and the subpolar jet may reappear. Apart from this possible distortion of the high latitude flow due to the absence of wavenumbers 1 and 2, we suggest that the climatic responses of the 2-wave 3-6 model to small perturbations in external parameters should be a good approximation to those of the untruncated two-level model.

c. *A note of caution*

The model used for this study exhibits a very peculiar behavior in certain cases. In the moist and dry 1-wave models with $m\geq 8$, a reasonable circulation develops initially, resembling the circulations in the 1-wave models with $m\leq 7$ described above, but after several hundred days of integration the eddy kinetic energy very slowly begins to decay, temperatures drift toward radiative equilibrium, surface winds decrease in strength, and the subtropical jets drift slowly equatorward. Various experiments were performed with different subgrid scale mixing and time finite-differencing in trying to understand this behavior. We found, surprisingly, that if we changed the procedure for convective adjustment by relaxing the fields to their adjusted values rather than adjusting instantaneously, these models quickly return to statistically steady states resembling those described above. The model's eddies are evidently incapable of maintaining their accustomed structure in the presence of very vigorous stirring, the stirring due to the adjustment being more vigorous in the presence of the smaller waves with their larger vertical motions.

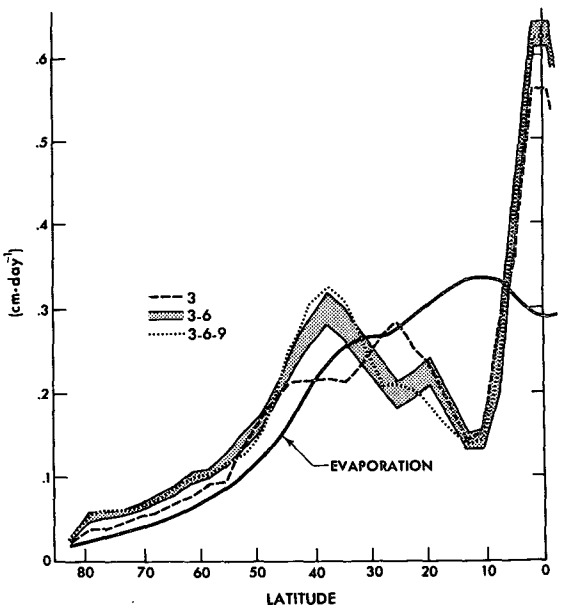

FIG. 17. Time-averaged precipitation in the 1-, 2-, and 3-wave experiments, and the evaporation rate in the 2-wave experiment, the sensitivity of the evaporation to spectral truncation being small.

Comparing a variety of experiments with different relaxation times, we found that those models which do not produce such a "drift" when the adjustment is instantaneous exhibited no appreciable sensitivity to the procedure used for the convective adjustment. In the other models, there seemed to be a critical relaxation time ($\lesssim$12 h) sufficient to bring the model back to its "realistic" climate.

None of the 1- or 2-wave models discussed in the previous sections exhibited this peculiar behavior. However, the 3-wave, 3-6-9 moist model did show signs of a very slow equatorward drift of the subtropical jets after about 500 days of integration. We therefore repeated this calculation, relaxing the convective adjustment with a time constant of 8 h. The

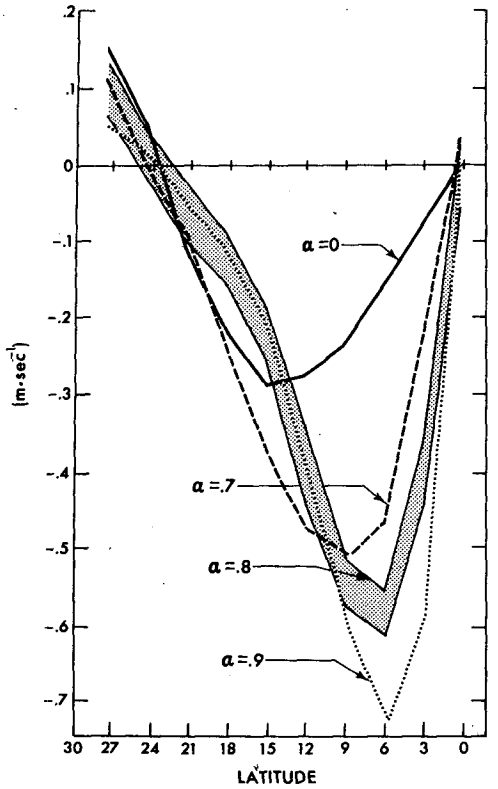

FIG. 18. The mean meridional circulation v_0 in the tropics of the 2-wave model with $\alpha=0$, 0.7, 0.8 and 0.9. Estimated standard deviations of 400-day averages are shown for $\alpha=0.8$.

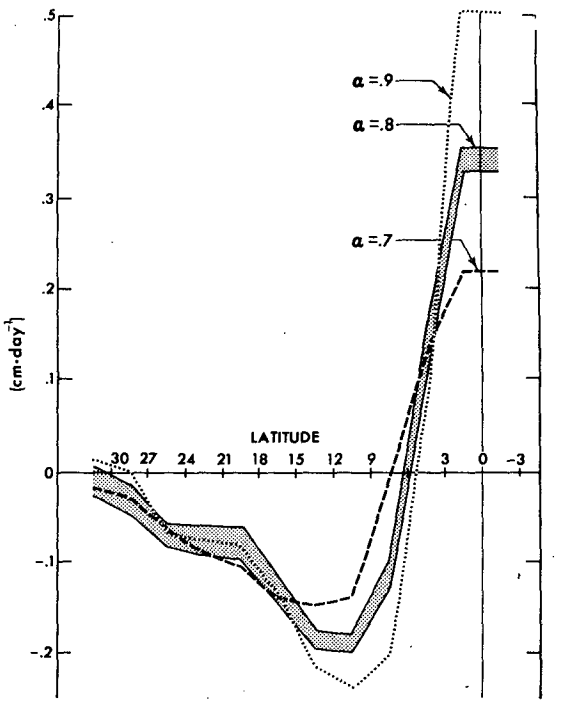

FIG. 19. Precipitation minus evaporation in the tropics of the 2-wave models with $\alpha=0.7$, 0.8 and 0.9.

model's climate was then stable, as best we could tell, for the full 700 days of integration, and these are the results we have described.

Being surprised that a version of the model could produce a plausible circulation for one and a half years of simulated time and then slowly begin to deteriorate, we wondered whether all of our integrations would eventually deteriorate if continued long enough. We therefore integrated the 1-wave $m=6$ "dry" model for 2400 days and found no evidence of such a "drift." The climatic statistics obtained from the 2000–2400 day period were nearly identical to those from the 300–700 day period.

6. The precipitation criterion

The moist integrations discussed in the previous sections were all performed with a precipitation criterion α of 0.8, that is, the mixing ratio in the lower layer was not allowed to exceed

$$0.8r_s=0.8(2Ac_p\hat{\Theta}_{\text{crit}}(\bar{T})/L).$$

We now examine the sensitivity of the model's climates to the value of the parameter α, using the 2-wave 3-6 model. Averages are again taken over the final 400 days of 700 day integrations.

The mean meridional circulations with $\alpha=0.7$, 0.8 and 0.9 as well as with $\alpha=0$ are shown in Fig. 18. (When $\alpha=0$, the atmosphere carries no water vapor, but $\hat{\Theta}$ is still maintained above $\hat{\Theta}_{\text{crit}}(\bar{T})$ by the convective adjustment.) $\hat{v}_0$ increases substantially as α increases, but only equatorward of 15°. The rest of the Hadley cell as well as the boundary between the Hadley and Ferrel cells is evidently controlled by the eddy fluxes and is relatively insensitive to the choice of α.

In Fig. 19 we plot precipitation minus evaporation, and in Fig. 20 the zonally averaged relative humidity, r_0/r_s, produced in the $\alpha=0.7$, 0.8 and 0.9 experiments. From Fig. 19 we learn that the ITCZ increases in strength and becomes more localized as α increases, to the point where the adequacy of 3° latitude meridional grid spacing becomes questionable. From Fig. 20 we learn that the model atmosphere is always raining at all longitudes at the equator, this being the only way that the time-averaged relative humidity can equal α. These tropical circulations are, therefore, effectively zonally symmetric and steady.

As discussed in Section 2b, in the limit $\alpha\rightarrow 1$ such a steady circulation would transport no energy out of the ITCZ. When we do try to obtain a statistically steady state for the model with $\alpha=1$, we find that upward motion becomes localized at one grid point and becomes quite variable, and an unacceptable amount of grid point noise develops in the model tropics. We have chosen the value $\alpha=0.8$ in order to avoid such

variability and in order to obtain an ITCZ which is at least marginally resolvable with our meridional grid.

The changes that occur in $\hat{v}_0$ and relative humidity when α is varied have opposite effects on the total energy transport by the Hadley cell. When α increases h_0 increases and therefore the equatorward transport of latent heat increases; but $\hat{v}_0$ also increases, which enhances the poleward flux of dry static energy more than it does the equatorward flux of latent heat since $2Ac_p\hat{\Theta}_0 > Lr_0$. We plot in Fig. 21 the total radiation surplus at the top of the model's tropical atmosphere (which must equal the divergence of total energy transport) for different values of α. The surplus is remarkably similar for the three values of α close to unity. What changes we do see in Fig. 21 are not systematic as α increases from 0.7 to 0.8 to 0.9. Even when $\alpha=0$, the circulation decreases in strength about the right amount to compensate for the total absence of latent heat transport. Since the outgoing longwave flux is, of course, a function of the atmospheric temperature, Fig. 21 implies that tropical temperatures are insensitive to α. This constancy of the total energy transport holds equally well in extratropical latitudes. In fact we find no systematic changes in temperature at any latitude as α is increased from 0.7 to 0.9.

It is not true, however, that the mid-latitude circulation is insensitive to *large* changes in α. In particular, the $\alpha=0$ model has almost twice as much eddy kinetic energy as the $\alpha=0.8$ model. Our point is simply that the midlatitude circulation and the tropical temperatures are not particularly sensitive to *small* changes in α when α is close to unity.

Evidently, the total energy transported by the model's Hadley cell, even in the vicinity of the equator, is not determined by the local dynamics of the tropical atmosphere. A useful picture of the relationship between the model's eddy fluxes and Hadley cell emerges from these experiments. The eddy fluxes can be thought of as determining the temperature of the model atmosphere down to 15° latitude, the role of the Hadley cell being to transport enough energy to maintain a small temperature difference between the equator and 15°. The strength of the Hadley cell near the equator is then determined by this required energy flux and the local vertical structure of the tropical atmosphere. [For a discussion of the role of the Hadley cell in maintaining small tropical temperature gradients, see Schneider (1977).]

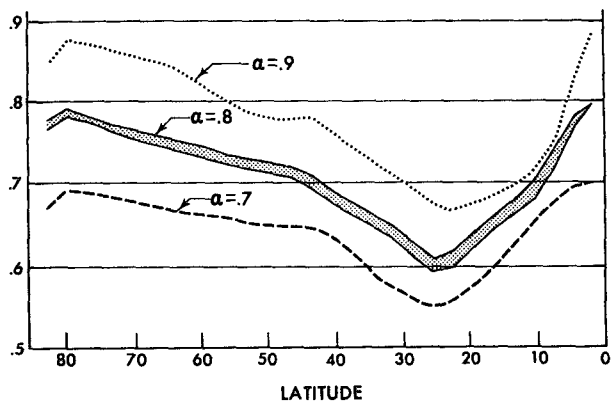

FIG. 20. The time-averaged relative humidity r_0/r_s predicted by the 2-wave models with $\alpha=0.7$, 0.8 and 0.9.

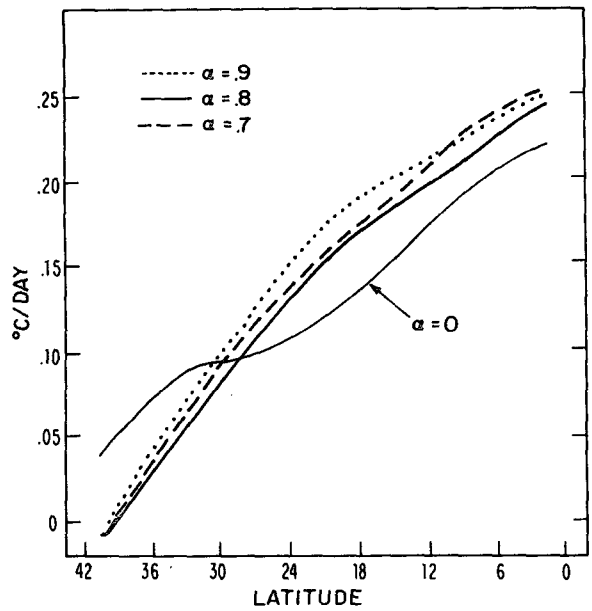

FIG. 21. The net radiation surplus at the top of the model's tropical atmosphere for $\alpha=0.7$, 0.8 and 0.9 and $\alpha=0$. The radiation surplus has been converted into a vertically averaged heating rate (1°C day^{-1} = 116 W m^{-2}). Estimated standard deviations of 400-day averages are of the order of 0.005°C day^{-1}.

On the basis of these experiments and this qualitative picture, we would argue that the arbitrariness involved in the choice of a precipitation criterion and, for that matter, the arbitrary character of the convective adjustment itself, are of no great significance for the model's climatic responses, except for those features which depend on the strength of the Hadley cell equatorward of 15°.

7. The maintenance of the model's static stability

We have developed two versions of this model—moist and dry—so as to be able to study climatic responses in atmospheres in which the static stability is maintained in two distinctly different ways. We discuss the balances maintaining the static stabilities in the two-wave $m=3$, 6 moist and dry models in this section. The discussion serves to emphasize a possible serious deficiency in two-level climate models.

The time-averaged, zonally averaged values of $\hat{\Theta}_0$ in these two experiments are shown in Fig. 22. Also shown is the stability of a moist adiabat $\hat{\Theta}_{crit}(\bar{T})$

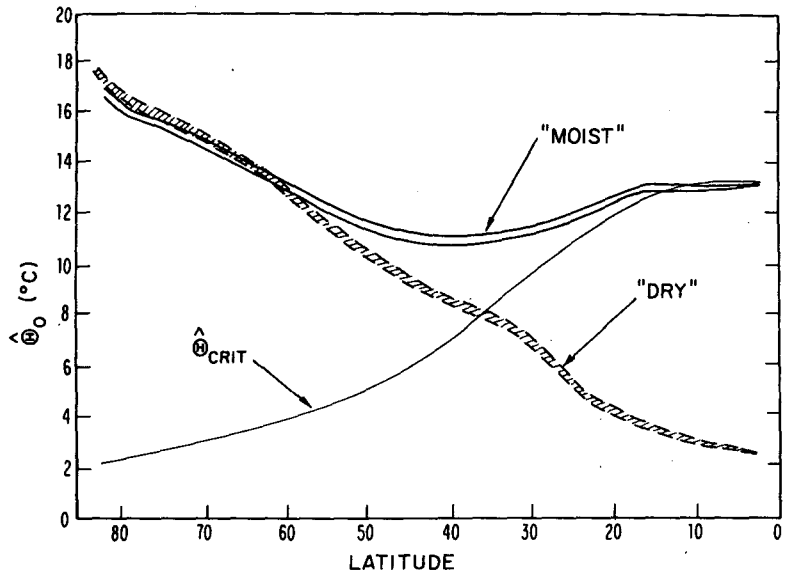

FIG. 22. $\hat{\Theta}_0$ maintained in the 2-wave, $m=3$, 6 moist and dry models, and the static stability of a moist adiabat $\hat{\Theta}_{crit}$ with the same mean atmospheric temperature as that produced in the moist integration.

evaluated using the mean atmospheric temperatures obtained from the moist integration.

Referring to (1) we divide the various terms contributing to $\partial\hat{\Theta}_0/\partial t$ in the moist model into:

1) The large-scale dynamical contribution

$$-\frac{1}{a\cos(\theta)}\frac{\partial}{\partial\theta}[\cos(\theta)\bar{v}_0\bar{\Theta}_0]-\omega_0\bar{\Theta}_0 \qquad \text{MMC}$$

$$-2\,\mathrm{Re}\sum_m \omega_m\bar{\Theta}_m^* \qquad \text{Vertical eddies}$$

$$-\frac{2\,\mathrm{Re}}{a\cos(\theta)}\sum_m\frac{\partial}{\partial\theta}[\cos(\theta)\widehat{v_m\Theta_m^*}] \qquad \text{Horizontal eddies.}$$

2) The radiative contribution

$$\frac{1}{c_p}\left(\frac{\hat{p}_*}{p}\right)^\kappa Q_0^{\mathrm{rad}}.$$

3) The remainder

$$-\frac{1}{2c_p}\left(\frac{p_*}{p_2}\right)^\kappa LP \qquad \text{Precipitation}$$

$$-\frac{1}{2c_p}\left(\frac{p_*}{p_2}\right)^\kappa Q^{\mathrm{sh}} \qquad \text{Sensible heating}$$

$$+\frac{A}{c_p}Q^{\mathrm{conv}} \qquad \text{Convective adjustment}$$

$$+\frac{1}{c_p}\left(\frac{\hat{p}_*}{p}\right)^\kappa Q_0^{\mathrm{diss}} \qquad \text{Diffusion.}$$

The upper part of Fig. 23 depicts the balance between these three groups of terms. In the lower part of Fig. 23 the contribution of the large scale dynamics is split into its three parts. In Fig. 24 we have divided the terms listed under 3) into the effects of evaporation plus sensible heating,

$$-\frac{1}{2c_p}\left(\frac{p_*}{p_2}\right)^\kappa(Q^{\mathrm{sh}}+LW^{\mathrm{evap}})$$

precipitation minus evaporation,

$$-\frac{1}{2c_p}\left(\frac{p_*}{p_2}\right)^\kappa L(P-W^{\mathrm{evap}}),$$

and convective adjustment. (The effect of diffusion is everywhere less than 0.04°C day^{-1} and is not plotted.) Since evaporation plus sensible heating must balance the net radiation at the surface, the combination of this term with the direct radiative heating in 2) should be considered the full "radiative" effect on the model's stability.

The distinctive characteristics of the stability balances in high, middle and low latitudes are evident from these figures. In high latitudes, the balance is between radiative stabilization and destabilization by the horizontal eddy flux of potential temperature. In mid-latitudes, the vertical eddy flux becomes a dominant feature of the balance, cooperating with radiative fluxes and convective adjustment in balancing the strong heating from below which, in turn, is enhanced considerably by moisture convergence in the lower layer. Near the equator, the dominant balance is between latent heat release and convective adjustment.

Fig. 25 describes the contributions to $\partial\hat{\Theta}_0/\partial t$ in the dry model. The stabilization due to convection is now that due to dry convective adjustment. The sum of the radiative stabilization and the destabilization due to the surface fluxes can again be thought of as the full radiative effect.

In neither model are the details of this balance of any importance for understanding the value of $\hat{\Theta}_0$ in the tropics. As discussed in Section 6, it is always raining (and convecting) at the equator in the moist case, so that $\hat{\Theta}_0 \approx \hat{\Theta}_{crit}$ as shown in Fig. 22, while $\hat{\Theta}_0 \approx \hat{\Theta}_{min} \equiv 2.5°C$ near the equator in the dry case. It is noteworthy that the eddies in the dry case are incapable of preventing the occurrence of dry convection equatorward of 30°.

The midlatitude stability balance in the moist case is rather complicated in that vertical fluxes due to the resolved large-scale eddies and those due to the moist convective adjustment are both important. It is here that comparison with the dry model should be of most interest. We find, in fact, that the midlatitude (30–45°) stability in the dry case is maintained by the large-scale vertical eddy fluxes. However, the magnitude of this flux has not increased substantially over that in the moist experiment and $\hat{\Theta}_0$ at the point of maximum flux (30°) is only half of its value in the moist case. A comparison of the horizontal and vertical fluxes reveals that the ratio of the mixing slope for potential temperature to the time-averaged isentropic slope is much larger in the moist than in the dry experiment, presumably because latent heat release enhances vertical motions—a point we shall return to in the discussion of eddy flux parameterizations in the second part of this study.

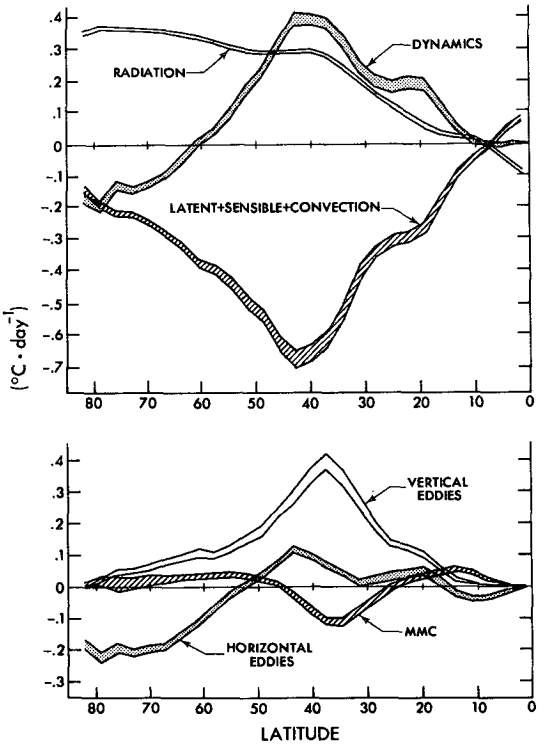

FIG. 23. Upper figure: $\partial\hat{\Theta}_0/\partial t$ due to radiation, resolved dynamics, and sum of all other processes, in the 2-wave, $m=3$, 6 moist model. Lower figure: $\partial\hat{\Theta}_0/\partial t$ due to resolved dynamics split into three parts, as described in text. Estimated variances of 400 day averages are shown for all terms.

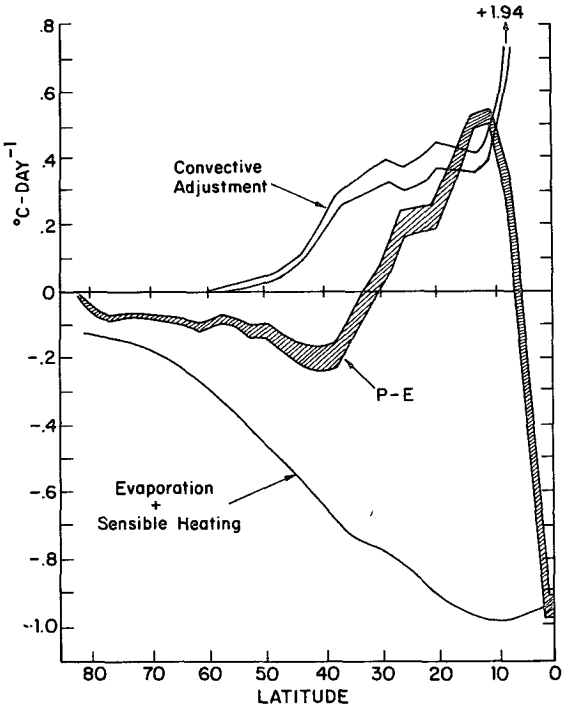

FIG. 24. $\partial\Theta_0/\partial t$ due to moist convective adjustment, precipitation minus evaporation ($P-E$), and evaporation plus sensible heating, in the 2-wave "moist" model. The estimated standard deviation for evaporation plus sensible heating is too small to be clearly visible.

The character of the stability balance in high latitudes is of particular interest. Neither the moist nor the dry model requires large-scale dynamical fluxes to maintain $\hat{\Theta}_0 > 0$ in high latitudes. In fact the net dynamical effect is destabilizing. There are, admittedly, net downward radiative fluxes at the surface balanced by upward sensible and latent heat fluxes, but the heating due to these surface fluxes is spread through the lower half of the atmosphere, and the resulting destabilization is then too small to counteract the stabilization due to long wave cooling in the lower layer. If the model's temperature profile were not constrained in the manner required by the 2-level approximation and if the heating due to surface fluxes were deposited near the ground, one might expect at least the lower troposphere to become unstable. If the model were also capable of describing eddies of sufficiently small vertical scale, such eddies might then contribute to the stabilization of the lower troposphere in high latitudes.

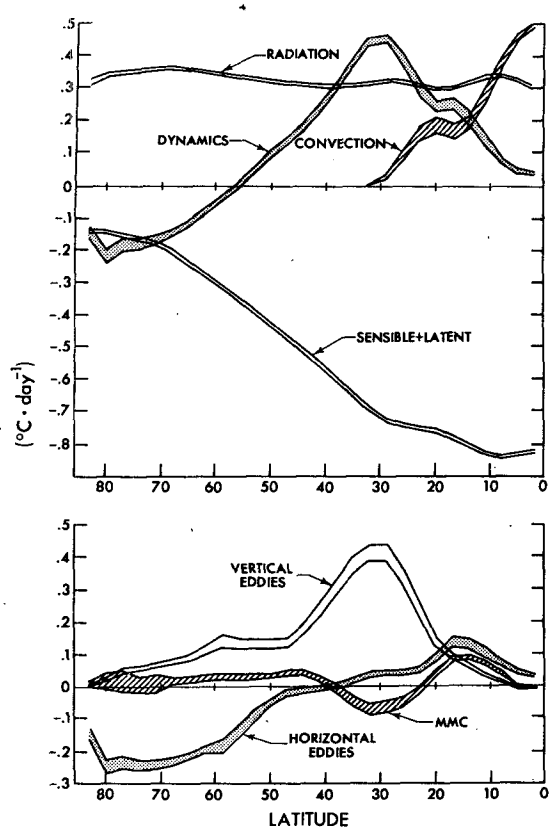

FIG. 25. Upper figure: $\partial\hat{\Theta}_0/\partial t$ due to radiation, resolved dynamics, dry convective adjustment, and surface fluxes in the 2-wave dry model. Lower figure: $\partial\hat{\Theta}_0/\partial t$ due to resolved dynamics split into three parts.

It is possible, therefore, that such a two-level model does not properly describe the interaction of radiation and dynamics in high latitudes.

8. Concluding remarks

We have described a particular two-level atmospheric model designed for the study of the atmosphere's gross response to small perturbations in external parameters. The model does produce a circulation resembling that of the earth's atmosphere and is at least two orders of magnitude more efficient than other two-level primitive equation models in use for climatic sensitivity studies (one order of magnitude for the zonal spectral truncation and another for the semi-implicit time step). We have tried, in this paper, to stress those features of the model which might limit its utility:

- Our choice of spectral truncation, zonal wavenumbers 3 and 6 plus the zonal flow, is not based on any systematic approximations to the untruncated model. The close similarity between the 2-wave $m=3, 6$ and 3-wave $m=3, 6, 9$ models suggests, however, that this truncation does not result in serious distortion of the zonally averaged circulation.
- Through our choice of a "precipitation criterion" we control the strength of the model's Hadley cell equatorward of 15°. Climatic responses of those parts of the system dependent on the strength of this part of the Hadley cell should clearly be viewed with scepticism. However, we find that this arbitrariness does not affect the extratropical circulation, or for that matter, the total energy transported by the Hadley cell or the tropical temperatures.
- Of most concern is the two-level approximation itself. The distortions resulting from the restriction to a fixed large vertical scale for all eddies and for the zonal temperature and wind structures are difficult to estimate.
- In addition, there is no doubt that the model's statistically steady states do depend somewhat on the character of its dissipative mechanisms—subgrid-scale mixing and surface drag—as well as on the meridional finite-differencing. We have not investigated this dependence systematically. Our calculations can only be of interest to the extent that explanations exist for the model's qualitative behavior which do not depend on these details. Our goal in analyzing this sort of model is to develop such explanations, and not to simulate the details of the observed climate or to obtain quantitative estimates of climatic sensitivity. We hope to convince the reader of the value of such a model in forthcoming papers.

Acknowledgments. We thank Syukoro Manabe and Joseph Smagorinsky for their guidance throughout this work. Computations were performed on the Texas Instruments Advanced Scientific Computer at the Geophysical Fluid Dynamics Laboratory. The assistance of the GFDL computer staff and scientific illustration group is gratefully acknowledged. Support was provided through NOAA Grant 04-3-00233 and National Science Foundation Grant GA-40341.

APPENDIX

Model Numerics

a. Meridional finite-differencing

Let $\theta_j, j=1, N$ be the latitudes of the integral $(\hat{a},\Theta,r)$ and $\theta_{j+\frac{1}{2}}$, $j=0, N$ the latitudes of the half-integral $(\hat{v},\psi,\zeta)$ points. We define

$$\Delta \equiv \theta_{j+1}-\theta_j=\theta_{j+\frac{1}{2}}-\theta_{j-\frac{1}{2}},$$

$$c_{j+\frac{1}{2}} \equiv \cos(\theta_{j+\frac{1}{2}}),$$

$$f_j \equiv 2\Omega \sin(\theta_j),$$

$$t_j \equiv -2(c_{j+\frac{1}{2}}-c_{j-\frac{1}{2}})/\Delta(c_{j+\frac{1}{2}}+c_{j-\frac{1}{2}}).$$

Let a tilde denote an average over two neighboring grid points and let a δ denote the meridional derivative

$(1/a)(\partial/\partial\theta)$ with two neighboring grid points, i.e.,

$$\tilde{\hat{v}}_{0,j}\equiv\tfrac{1}{2}(\hat{v}_{0,j+\frac{1}{2}}+\hat{v}_{0,j-\frac{1}{2}}),$$
$$\tilde{\bar{u}}_{0,j+\frac{1}{2}}\equiv\tfrac{1}{2}(\bar{u}_{0,j+1}+\bar{u}_{0,j}),$$
$$\delta(\hat{v}_0)_j\equiv(1/a\Delta)(\hat{v}_{0,j+\frac{1}{2}}-\hat{v}_{0,j-\frac{1}{2}}),$$
$$\delta(\tilde{c}\tilde{\hat{v}}_m)_{j+\frac{1}{2}}\equiv(1/a\Delta)(\tilde{c}_{j+1}\tilde{\hat{v}}_{m,j+1}-\tilde{c}_j\tilde{\hat{v}}_{m,j}),\text{ etc.}$$

The streamfunction is obtained from the vorticity by solving the equation

$$\zeta_{m,j+\frac{1}{2}}=\frac{1}{c_{j+\frac{1}{2}}}\delta[\tilde{c}\delta(\psi_m)]_{j+\frac{1}{2}}-\frac{m^2}{a^2c_{j+\frac{1}{2}}^2}\psi_{m,j+\frac{1}{2}}\quad(m\neq0)$$

with the boundary conditions

$$\psi_{m,\frac{1}{2}}=\psi_{m,N+\frac{1}{2}}=0.$$

The barotropic u-velocity at integral grid points and the barotropic v-velocity at half-integral points are then obtained from

$$\bar{u}_{m,j}\equiv-\delta(\psi_m)_j,$$
$$\bar{v}_{m,j+\frac{1}{2}}\equiv\frac{im}{ac_{j+\frac{1}{2}}}\psi_{m,j+\frac{1}{2}}.$$

The vertical velocity at integral grid points is defined by

$$\omega_{m,j}\equiv-\frac{1}{\tilde{c}_j}\delta(c\hat{v}_m)_j-\frac{im}{a\tilde{c}_j}\tilde{\hat{u}}_{m,j}.$$

We also require the following auxiliary variables

$$\langle\bar{u}_m\rangle_{j+\frac{1}{2}}\equiv-\delta(\tilde{\psi}_m)_{j+\frac{1}{2}},$$
$$\langle\bar{v}_m\rangle_j\equiv\frac{im}{a\tilde{c}_j}\tilde{\psi}_{m,j},\qquad j=2,\,N-1,$$
$$\equiv0,\qquad j=1\text{ and }j=N,$$
$$\langle u_{1,m}\rangle_{j+\frac{1}{2}}\equiv\langle\bar{u}_m\rangle_{j+\frac{1}{2}}+\tilde{\hat{u}}_{m,j+\frac{1}{2}},$$
$$\langle u_{2,m}\rangle_{j+\frac{1}{2}}\equiv\langle\bar{u}_m\rangle_{j+\frac{1}{2}}-\tilde{\hat{u}}_{m,j+\frac{1}{2}},$$

(and similarly for $\langle v_{1,m}\rangle_j$, $\langle v_{2,m}\rangle_j$) and

$$\langle\omega_m\rangle_{j+\frac{1}{2}}\equiv-\frac{1}{c_{j+\frac{1}{2}}}\delta(\tilde{c}\tilde{\hat{v}})_{j+\frac{1}{2}}-\frac{im}{ac_{j+\frac{1}{2}}}\tilde{\hat{u}}_{m,j+\frac{1}{2}}.$$

Then

$$\frac{\partial\hat{u}_{m,j}}{\partial t}=\frac{f_j}{c_j}(\widetilde{c\hat{v}_m})_j-\frac{imc_pB}{a\tilde{c}_j}\bar{\Theta}_{m,j}+\sum_{m'm''}{}'[\hat{M}_j(m',m'')-\omega_{m',j}\bar{u}_{m'',j}]$$

$$\frac{\partial\hat{v}_{m,j+\frac{1}{2}}}{\partial t}=-(f\widetilde{\hat{u}_m})_{j+\frac{1}{2}}-c_pB\delta(\bar{\Theta}_m)_{j+\frac{1}{2}}+\sum_{m'm''}{}'[\hat{N}_{j+\frac{1}{2}}(m',m'')-\langle\omega_{m'}\rangle_{j+\frac{1}{2}}\bar{v}_{m'',j+\frac{1}{2}}],$$

$$\frac{\partial\zeta_{m,j+\frac{1}{2}}}{\partial t}=-\frac{2im\Omega}{a^2}\psi_{m,j+\frac{1}{2}}+\sum_{m'm''}{}'\left\{\frac{im}{ac_{j+\frac{1}{2}}}\bar{N}_{j+\frac{1}{2}}(m',m'')-\frac{1}{c_{j+\frac{1}{2}}}\delta[\tilde{c}\bar{M}(m',m'')]_{j+\frac{1}{2}}\right\}\quad(m\neq0),$$

$$\frac{\partial\bar{u}_{0,j}}{\partial t}=\sum_m\bar{M}_j(m,-m),$$

$$\frac{\partial\bar{\Theta}_{m,j}}{\partial t}=\sum_{m'm''}{}'\bar{S}_j(m',m''),$$

$$\frac{\partial\hat{\Theta}_{m,j}}{\partial t}=\sum_{m'm''}{}'[\hat{S}_j(m',m'')-\omega_{m',j}\bar{\Theta}_{m'',j}],$$

$$\frac{\partial r_{m,j}}{\partial t}=\sum_{m'm''}{}'\left[-\frac{1}{\tilde{c}_j}\delta(cv_{2,m'}\tilde{r}_{m''})_j-\frac{im}{a\tilde{c}_j}u_{2,m',j}r_{m'',j}\right],$$

where the primed summation is defined in Eq. (2) in the text, and where

$$M_{k,j}(m',m'')\equiv-\frac{1}{\tilde{c}_j^2}\delta(c^2v_{k,m'}\tilde{u}_{k,m''})_j-\frac{im}{a\tilde{c}_j}u_{k,m',j}u_{k,m'',j},$$

$$N_{k,j+\frac{1}{2}}(m',m'')\equiv-\frac{1}{c_{j+\frac{1}{2}}}\delta(\tilde{c}\langle v_{k,m'}\rangle\tilde{v}_{k,m''})_{j+\frac{1}{2}}-\frac{im}{ac_{j+\frac{1}{2}}}\langle u_{k,m'}\rangle_{j+\frac{1}{2}}v_{k,m'',j+\frac{1}{2}}-\frac{1}{a}\widetilde{(tu_{k,m'})}_{j+\frac{1}{2}}\tilde{u}_{k,m'',j+\frac{1}{2}},$$

$$S_{k,j}(m',m'')\equiv-\frac{1}{\tilde{c}_j}\delta(cv_{k,m'}\bar{\Theta}_{k,m''})_j-\frac{im}{a\tilde{c}_j}u_{k,m',j}\Theta_{k,m'',j};\qquad k=1,2.$$

For the finite-difference analogs of the conserved quantities mentioned in the text, and for a discussion of how these conservation properties were used to help design the finite-differencing scheme, we refer to Held (1976).

b. Time finite-differencing

Schematically, we use a time finite-differencing of the following form

$$(\rho^{n+1}-\rho^{n-1})/2\Delta t=(\text{advection})^n+(1-\xi)(\text{inertio-gravity})^{n-1}+\xi(\text{inertio-gravity})^{n+1},$$

where the superscript refers to the time step. If $\xi=\frac{1}{2}$, the amplitude of inertio-gravitational oscillations is conserved in time. If $\xi>\frac{1}{2}(<\frac{1}{2})$ inertio-gravitational oscillations are damped (amplified). We choose $\xi=\frac{1}{2}$ in the eddy ($m\neq 0$) equations but find it very useful to damp zonally symmetric inertio-gravity waves strongly by choosing $\xi=1$ in the zonal equations. In the absence of this damping mechanism, zonally symmetric equatorial oscillations grow to unrealistic amplitudes ($\sim$10 m s^{-1}) after several hundred days of integration. (Unrealistic, that is, when compared with atmospheric observations; it is entirely possible that the true solutions to the two-level primitive equation model actually are dominated by trapped equatorial oscillations.)

Because of the surface pressure constraint, there are no gravity waves in the barotropic mode. Further, because of the vertical finite-differencing, the pressure gradients driving the baroclinic mode are functions only of $\bar{\Theta}_m$ and not of the static stability $\hat{\Theta}_m$. Therefore, the equations for $\hat{\Theta}_m$ and ζ_m (as well as r_m) involve only explicit terms (the β-effect term in $\partial\zeta_m/\partial t$ is treated explicitly). The equations for $\hat{u}_m$, $\hat{v}_m$ and $\bar{\Theta}_m$ for each m are coupled by the implicit terms.

We write $\hat{\Theta}_0=\Pi+\hat{\Theta}_0'$, where Π is independent of latitude, so that

$$-\frac{1}{\tilde{c}_j}\delta(c\hat{v}_m\tilde{\hat{\Theta}}_0)_j-\frac{im}{ac_j}\hat{u}_{m,j}\hat{\Theta}_{0,j}$$
$$=-\frac{1}{\tilde{c}_j}\delta(c\hat{v}_m\tilde{\hat{\Theta}}_0')_j-\frac{im}{ac_j}\hat{u}_{m,j}\hat{\Theta}_{0,j}+\Pi\omega_{m,j}.$$

The only term treated implicitly in the equation for $\partial\bar{\Theta}_{m,j}/\partial t$ is $\Pi\omega_{m,j}$. As long as Π remains larger than Θ_0' we expect the scheme to be computationally stable (Kurihara, 1965). We choose $\Pi=20$°C in all experiments. Using the notation

$$\delta_t\hat{u}_{m,j}\equiv(\hat{u}_{m,j}^{n+1}-\hat{u}_{m,j}^{n-1})/(2\Delta t)$$

the relevant equations can be written in the form

$$\delta_t\hat{u}_{m,j}=2\Delta t\xi\left[\frac{f_j}{2\tilde{c}_j}(c_{j+\frac{1}{2}}\delta_t\hat{v}_{m,j+\frac{1}{2}}-c_{j-\frac{1}{2}}\delta_t\hat{v}_{m,j-\frac{1}{2}})-\frac{imc_pB}{a\tilde{c}_j}\delta_t\bar{\Theta}_{m,j}\right]+X_{m,j},$$

$$\delta_t\hat{v}_{m,j+\frac{1}{2}}=2\Delta t\xi\left[-\tfrac{1}{2}(f_{j+1}\delta_t\hat{u}_{m,j+1}+f_j\delta_t\hat{u}_{m,j})-\frac{c_pB}{a\Delta}(\delta_t\bar{\Theta}_{m,j+1}-\delta_t\bar{\Theta}_{m,j})\right]+Y_{m,j+\frac{1}{2}},$$

$$\delta_t\bar{\Theta}_{m,j}=2\Delta t\xi\Pi\left[-\frac{1}{a\tilde{c}_j\Delta}(c_{j+\frac{1}{2}}\delta_t\hat{v}_{m,j+\frac{1}{2}}-c_{j-\frac{1}{2}}\delta_t\hat{v}_{m,j-\frac{1}{2}})-\frac{im}{a\tilde{c}_j}\delta_t\hat{u}_{m,j}\right]+Z_{m,j},$$

where X, Y and Z represent all terms treated explicitly (which include all heating and frictional terms). These equations can be reduced to one tri-diagonal form

$$\mathcal{P}_{j+\frac{1}{2}}\delta_t\hat{v}_{m,j+\frac{3}{2}}+Q_{j+\frac{1}{2}}\delta_t\hat{v}_{m,j+\frac{1}{2}}+\mathcal{R}_{j+\frac{1}{2}}\delta_t\hat{v}_{m,j-\frac{1}{2}}=T_{j+\frac{1}{2}}$$

easily solved for $\delta_t\hat{v}_m$ with the boundary conditions

$$\delta_t\hat{v}_{m,\frac{1}{2}}=\delta_t\hat{v}_{m,N+\frac{1}{2}}=0;$$

$\delta_t\bar{\Theta}_m$ and $\delta_t\hat{u}_m$ are then easily obtained from the formulas above.

To remedy a very weak splitting, a single time step of the form

$$(\rho^{n+1}-\rho^n)/\Delta t=(\text{advection})^n+(1-\xi)(\text{inertio-gravity})^n+\xi(\text{inertio-gravity})^{n+1}$$

is taken every 50 steps. Δt in our integrations varies from 1 to 2 hours, depending partly on the presence or absence of strong subpolar jets.

REFERENCES

Arakawa, A., and V. R. Lamb, 1977: Computational design of the basic dynamical processes of the UCLA general circulation model. *Methods of Computational Physics*, Vol. 17, J. Chang, Ed., Academic Press, 173–265.

Bates, J. R., 1970: Dynamics of disturbances on the intertropical convergence zone. *Quart. J. Roy. Meteor. Soc.*, **96**, 677–701.

Bryan, K., 1969: A numerical method for the study of the circulation of the world ocean. *J. Comput. Phys.*, **4**, 347–376.

Budyko, M. I., 1969: The effect of solar radiation variations on the climate of the earth. *Tellus*, **21**, 611–619.

Gates, W. L., 1976: The numerical simulation of ice-age climate with a global general circulation model. *J. Atmos. Sci.*, **33**, 1844–1873.

Held, I. M., 1975: Momentum transport by quasi-geostrophic eddies. *J. Atmos. Sci.*, **32**, 1494–1497.

——, 1976: The tropospheric lapse rate and climatic sensitivity. Ph.D. thesis, Princeton University, 217 pp.

Kurihara, Y., 1965: On the use of implicit and iterative methods for the time integration of the wave equation. *Mon. Wea. Rev.*, **93**, 33–49.

——, 1970: A statistical-dynamical model of the general circulation of the atmosphere. *J. Atmos. Sci.*, **27**, 847–870.

Kwizak, M., and A. J. Robert, 1971: A semi-implicit scheme for grid point atmospheric models of the primitive equations. *Mon. Wea. Rev.*, **99**, 32–36.

Leith, C. E., 1973: The standard error of time-average estimates of climatic means. *J. Appl. Meteor.*, **12**, 1066–1069.

Lorenz, E. N., 1960: Energy and numerical weather prediction. *Tellus*, **12**, 364–373.

Manabe, S., and R. F. Strickler, 1964: Thermal equilibrium of the atmosphere with a convective adjustment. *J. Atmos. Sci.*, **21**, 361–385.

——, and R. Wetherald, 1967: Thermal equilibrium of the

atmosphere with a given distribution of relative humidity. *J. Atmos. Sci.*, **24**, 241–259.

——, D. G. Hahn, and J. L. Holloway, 1974: The seasonal variation of the tropical circulation as simulated by a global model of the atmosphere. *J. Atmos. Sci.*, **31**, 43–83.

Moura, A. D., and P. H. Stone, 1976: The effects of spherical geometry on baroclinic instability. *J. Atmos. Sci.*, **33**, 602–616.

Oort, A. H., and J. P. Peixoto, 1974: The annual distribution of atmospheric energy on a planetary scale. *J. Geophys. Res.*, **79**, 2149–2159.

Phillips, N. A., 1951: A simple three-dimensional model for the study of large-scale extratropical flow patterns. *J. Meteor.*, **8**, 381–394.

Ramanathan, V., 1976: Radiative transfer within the earth's troposphere and stratosphere: A simplified radiative-convective model. *J. Atmos. Sci.*, **33**, 1330–1346.

Rodgers, C. D., and C. D. Walshaw, 1966: The computation of infrared cooling rates in planetary atmospheres. *Quart. J. Roy. Meteor. Soc.*, **92**, 67–92.

Schneider, E. K., 1977: Axially symmetric steady-state models of the basic state for instability and climate studies. Part II. Nonlinear calculations. *J. Atmos. Sci.*, **34**, 280–297.

Sela, J., and A. Wiin-Nielsen, 1971: Simulation of the atmospheric annual energy cycle. *Mon. Wea. Rev.*, **99**, 460–468.

Sellers, W. D., 1969: A global climate model based on the energy balance of the earth-atmosphere system. *J. Appl. Meteor.*, **8**, 392–400.

Smagorinsky, J., 1963: General circulation experiments with the primitive equations. I. The basic experiment. *Mon. Wea. Rev.*, **91**, 99–164.

Stone, P. H., 1972: A simplified radiative-dynamical model for the static stability of rotating atmospheres. *J. Atmos. Sci.*, **29**, 405–418.

Stone, H. M., and S. Manabe, 1968: Comparison among various numerical models designed for computing infrared cooling. *Mon. Wea. Rev.*, **96**, 735–741.

Suarez, M. J., 1976: An evaluation of the astronomical theory of the ice ages. Ph.D. thesis, Princeton University, 108 pp.

Webster, P. J., and K. M. W. Lau, 1977: A simple ocean-atmosphere climate model: Basic model and a simple experiment. *J. Atmos. Sci.*, **34**, 1063–1084.

Wetherald, R. T., and S. Manabe, 1975: The effects of changing the solar constant on the climate of a general circulation model. *J. Atmos. Sci.*, **32**, 2044–2059.